arXiv:1204.0086v1 [math.NA] 31 Mar 2012

A viscoplasticity model with an enhanced control of the yield surface distortion

A. V. Shutov, J. Ihlemann

Chemnitz University of Technology, Chair of Solid Mechanics, Chemnitz, Germany

---

Abstract

A new model of metal viscoplasticity, which takes combined isotropic, kinematic, and distortional hardening into account, is presented. The basic modeling assumptions are illustrated using a new two-dimensional rheological analogy. This demonstrative rheological model is used as a guideline for the construction of constitutive relations. The nonlinear kinematic hardening is captured using the well-known Armstrong-Frederick approach. The distortion of the yield surface is described with the help of a so-called distortional backstress. A distinctive feature of the model is that any smooth convex saturated form of the yield surface which is symmetric with respect to the loading direction can be captured. In particular, an arbitrary sharpening of the saturated yield locus in the loading direction combined with a flattening on the opposite side can be covered. Moreover, the yield locus evolves smoothly and its convexity is guaranteed at each hardening stage. A strict proof of the thermodynamic consistency is provided. Finally, the predictive capabilities of the material model are verified using the experimental data for a very high work hardening annealed aluminum alloy 1100 Al.

Keywords: viscoplasticity, yield function, kinematic hardening, distortional hardening, rheology
2000 MSC: 74C10, 74S05

Nomenclature

α	distortion parameter, cf. (13), (26)
$\mathbf{X}_{\mathrm{k}}$, $\mathbf{X}_{\mathrm{d}}$	backstress and distortional backstress, respectively
R	isotropic hardening, cf. $(18)_4$
$\boldsymbol{\sigma}_{\mathrm{eff}}$	effective stress, cf. $(20)_1$

Preprint submitted to International Journal of Plasticity *February 22, 2013*

$\boldsymbol{R}_{\text{eff}}$	effective radial direction, cf. $(32)_2$
$\boldsymbol{\varepsilon}_{\text{i}}$, $\boldsymbol{\varepsilon}_{\text{e}}$	inelastic and elastic strains, respectively, cf. $(14)_1$
$\boldsymbol{\varepsilon}_{\text{ki}}$, $\boldsymbol{\varepsilon}_{\text{di}}$	dissipative parts of $\boldsymbol{\varepsilon}_{\text{i}}$, cf. $(14)_2$, $(14)_3$
$\boldsymbol{\varepsilon}_{\text{ke}}$, $\boldsymbol{\varepsilon}_{\text{de}}$	conservative parts of $\boldsymbol{\varepsilon}_{\text{i}}$, cf. $(14)_2$, $(14)_3$
λ_{i}	inelastic multiplier, cf. $(24)_2$
p	accumulated inelastic arc-length (Odqvist parameter), cf. $(24)_3$
s, s_{d}	internal variables of isotropic hardening, cf. $(14)_4$, (28)
θ	angle between $\boldsymbol{\sigma}^{\text{D}}_{\text{eff}}$ and $\mathbf{X}_{\text{d}}$, cf. $(20)_2$
f	overstress, cf. (10), (21)
$\bar{f}$	non-dimensional overstress, cf. (6)
$\text{El}(\bar{K}(\cdot, \alpha))$	non-dimensional elastic domain, cf. (2) and Fig. 3b
$\bar{K}(\theta, \alpha)$	non-dimensional yield stress function, cf. (5)
$\bar{K}^{\text{sat}}(\theta)$	non-dimensional saturated yield stress function
$\mathcal{D}(\vec{y}, A)$	distance between $\vec{y} \in \mathbb{R}^2$ and $A \subset \mathbb{R}^2$, cf. (3)

1. Introduction

Numerical simulation of complex metal forming operations is a powerful tool to reduce the development costs and to optimize the mechanical properties of a workpiece. For many polycrystalline metals, the initial yield surface can be approximated with sufficient accuracy by the conventional Huber-Mises yield condition which implies initial plastic isotropy. On the other hand, already very small plastic deformations may lead to a significant change of the yield surface compared to the initial state (Annin , 1978; Wegener and Schlegel , 1996; Dannemeyer , 1999; Steck et al. , 2001; Khan et al. , 2010a,b). It is well known that the residual stresses, springback, damage evolution, and failure are highly dependent on the accumulated plastic anisotropy of the material. In this work we concentrate on the *phenomenological* modeling of the plastic anisotropy with especial emphasis on the distortional hardening. A conventional approach to metal plasticity is used in the current study: we suppose that a unique yield surface exists and that the material behavior is purely elastic for stresses within the yield surface.[1]

---

[1] Alternatively, different unconventional concepts with numerous types of “yield” surfaces exist. The so-called “subloading surface models” (see Hashiguchi (1989) and references therein) allow to capture the plastic flow for stresses within the “yield” surface. Such approach allows to obtain a smooth transition from the elastic into the elasto-plastic

The state of the art phenomenological plasticity is a result of accumulated efforts made by generations of researchers. Unfortunately, little academic credit was given to the paper written by Prager (1935). Already in 1935, Prager combined the isotropic hardening of Odqvist type, the distortional hardening for the prediction of cross hardening effect, and the kinematic hardening for the Bauschinger effect. Interestingly, the idea of modeling the Bauschinger effect by the kinematic translation of the Huber-Mises yield surface in the stress space was taken by Prager from a conference talk given by A. Reuß a year before - in 1934!

Within the classical phenomenological model of Chaboche and Rousselier (1983a,b), the isotropic expansion and kinematic translation of the yield surface are considered, such that the yield surface is represented by a hypersphere in the deviatoric stress space.[2] Thus, the change of the form of the yield surface is neglected. Such models can be used to simulate the stress response under proportional loading. However, in general, the distortion of the yield surface has to be considered under nonproportional loading with abrupt change of the loading path. Such loading conditions are typical not only for multi-stage forming processes, but even for some single-stamping forming operations. In order to control the rotation of a hyperellipsoid which represents the yield surface withing a Hill-type theory[3], Baltov and Sawczuk (1964) introduced a polynomial representation of the corresponding 4th rank Hill-type anisotropy tensor in terms of the strain tensor. According to Betten (1976), 4th and 6th rank hardening tensors are postulated as functions of the plastic strain. Dafalias (1979) considered a general representation of the 4th rank tensor as a polynomial function of the plastic strain. In the paper by Helling and Miller (1987), the 4th rank Hill-type anisotropy tensor is assumed to be a function of two backstress-like tensors. In contrast to the above mentioned approaches, the approach of Helling allows to take the dependence on the strain path into account. For the same purpose, Rees (1984); Streilein (1997); Kowalsky (1999); Steck et al. (2001); Dafalias et. al. (2002); Feigenbaum and Dafalias (2007); Noman et. al. (2010);

---

range. Moreover, some models with a smooth stress response can be constructed using the concept of "bounding surface" (see, for instance, Dafalias and Popov (1975)).

[2] Such yield surface can be represented by a hypersphere in Ilyushin's space, as well (see Ilyushin (1954)).

[3] The original approach of Hill (1948) can be used to describe a certain *initial* plastic anisotropy, but not its evolution.

Dafalias and Feigenbaum (2011); Pietryga et. al. (2012) and others modified the Chaboche-Rousselier model introducing ordinary differential equations which describe the evolution of tensor-valued internal variables of higher order (typically 4th and 6th rank tensors). An alternative integral approach was presented by Danilov (1971). In the paper of Grewolls and Kreißig (2001), evolution equations for higher order tensors were formulated in integral form using the Danilov's approach. Both differential and integral approaches mentioned above allow to take the dependence of the hardening on the strain path. Kurtyka and Zyczkowski (1985, 1996) proposed a geometric approach in order to simulate a complex distortion of the yield surface.

The rigorous proof of convexity of the yield surface may become rather difficult, if the 4th rank tensors are used (Plesek et. al. , 2010). For instance, due to the complexity of the model presented by Pietryga et. al. (2012), the convexity of the yield surface was tested numerically by plotting its two-dimensional projection at different loading stages.

Probably, the most simple generalizations of the Chaboche-Rousselier model are based on the use of second-rank backstress-like tensors. Within this approach, the orientation of the yield surface follows the loading path such that the change of the loading direction leads to a reorientation of the yield surface with a certain time lag. A short overview concerning different approaches based on the use of backstress-like tensors is presented by Wegener and Schlegel (1996). In particular, within the model of Ortiz and Popov (1983), the size of the elastic domain along a radial line emanating from the origin of the yield surface depends on the angle θ between the effective deviatoric stress and the backstress direction. More precisely, the critical norm of the effective deviatoric stress is given by a Fourier cosine series of θ. Thus, an arbitrary yield surface which is symmetric with respect to the backstress direction can be approximated. On the other hand, the convexity of the yield surface imposes constraints on the Fourier coefficients. These constraints complicate the construction of practical material models, especially if the smooth evolution of the yield surface is intended. Another special case was considered by François (2001). Within this approach, certain egg-shaped yield surfaces can be modeled, such that the egg-axis is oriented along a backstress-like tensor $\mathbf{X}_{\mathrm{d}}$ and the degree of distortion is proportional to $\|\mathbf{X}_{\mathrm{d}}\|$. In particular, if Armstrong-Frederick type of hardening is used to describe the evolution of $\mathbf{X}_{\mathrm{d}}$, the distortion evolves in time smoothly. The thermodynamic consistency was numerically tested by François. Next, within the approach presented by Panhans (2006) as well as Panhans and Kreißig

(2006), the distortional hardening was captured with the help of a tensor-valued internal variable of the 2nd rank. The form of the yield surface is given by the so-called limaçon of Pascal. Within the approach of Panhans it can be easily guaranteed that the elastic domain is simply connected and convex. Later, in the paper of Shutov et al. (2011), a two-dimensional rheological model of distortional hardening was suggested, which implies the yield surface to be the the limaçon of Pascal. This rheological model was used to construct thermodynamically consistent constitutive equations of finite strain plasticity/viscoplasticity. In the paper by Feigenbaum and Dafalias (2008), an existing material model was simplified in a thermodynamically consistent manner such that second-rank backstress-like tensors are used only.

A relatively new concept of representative directions (see, for example, Freund et al. (2011)) allows to generalize a uniaxial material model to cover an arbitrary triaxial loading. In order to compute the stress response, a numerical integration on the sphere S^2 is required. This concept, if combined with a uniaxial phenomenological model of plasticity/viscoplasticity, can produce a new phenomenological model with some realistic distortional hardening effects. An interesting simplified approach to the description of plastic anisotropy was proposed by Barlat et. al. (2011). Interestingly, this approach does not include the concept of kinematic hardening explicitly, but some distortional effects can be captured. The simplified approach to distortional hardening, which was developed by Aretz (2008), does not include kinematic hardening as well. Further, we note that some models of crystal/polycrystal plasticity allow the description of the yield surface distortion in a natural way (cf. Rousselier et. al. (2010)). For instance, in the paper by Fang et al. (2011), the impact of microstructural hardening parameters on the form of the yield locus was analyzed in the finite strain context. It was shown that for reduced latent hardening the yield surface exhibits a larger curvature in the loading direction.

A new phenomenological model of metal plasticity is proposed in the current study. The main features of the current model are as follows:

(i) a *two-dimensional rheological motivation* of constitutive equations, which provides insight into main modeling assumptions;

(ii) nonlinear isotropic hardening of Voce type and nonlinear kinematic hardening of Armstrong-Frederick type;

(iii) *arbitrary* smooth convex yield surface for saturated distortional hardening, which is symmetric with respect to a backstress-like tensor $\mathbf{X}_\mathrm{d}$;

(iv) degree of yield surface distortion is proportional to $\|\mathbf{X}_\mathrm{d}\|$; *the convexity of the yield surface is guaranteed* at each hardening stage;

(v) normality flow rule; pressure-insensitive plasticity;

(vi) explicit formulation of the free energy density and *thermodynamic consistency*;

(vii) overstress type of viscoplasticity according to Perzyna rule.

In this paper, the temperature field is assumed to be constant in time and space.[4] The model is formulated for infinitesimal strains such that the extreme simplicity of the current approach is not obscured by the geometric nonlinearities. At the same time, the elegant technique of Lion (2000), which is based on the consideration of rheological analogies can be used to generalize the constitutive equations to finite strains (Helm , 2001; Shutov and Kreißig , 2008a; Henann and Anand , 2009; Vladimirov , 2010). As it was shown by Shutov et al. (2011), a similar technique can be implemented for two-dimensional rheological models, as well. Alternatively to the approach of Lion, the method of rheological models proposed by Palmow (1984) can be used to construct finite-strain constitutive relations.

We conclude the introduction with a few remarks regarding notation. The elements of $\mathbb{R}^2$ are denoted by $\vec{x}$, $\vec{y}$. The notations $\vec{x} \cdot \vec{y} := x_1 y_1 + x_2 y_2$ and $\|\vec{x}\| := \sqrt{\vec{x} \cdot \vec{x}}$ stand for the scalar product and the corresponding norm, respectively. A coordinate-free tensor setting in $\mathbb{R}^3$ is implemented (cf. Itskov (2007); Shutov and Kreißig (2008b)). Bold-faced symbols denote 1st- and 2nd-rank tensors in $\mathbb{R}^3$. Superimposed dot denotes the material time derivative: $\dot{x} = \frac{d}{dt} x$. The symbol " : " stands for the scalar product of two second-rank tensors

$$\mathbf{A} : \mathbf{B} := \mathrm{tr}(\mathbf{A} \cdot \mathbf{B}^\mathrm{T}).$$

---

[4] The model is formulated in a thermodynamically admissible manner. Therefore, its generalization to thermoplasticity is straight-forward. The equation of heat conduction can be derived directly from the energy balance, and an additional type of free energy (so-called "detached" free energy) can be introduced for better prediction of temperature evolution, cf. Shutov and Ihlemann (2011).

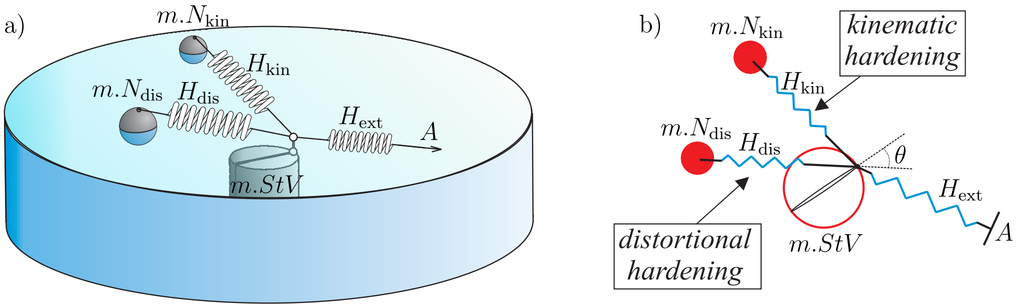

Figure 1: a) Two-dimensional rheological model is built up of a modified St.-Venant element ($m.StV$), Hooke-bodies H_{ext}, H_{kin}, H_{dis}, and modified Newton elements $m.N_{\text{kin}}$ and $m.N_{\text{dis}}$; b) Rheological model seen from above. The angle between the ($m.StV$)-axis and H_{dis} is denoted by θ.

This scalar product gives rise to the Frobenius norm as follows

$$\|\mathbf{A}\| := \sqrt{\mathbf{A} : \mathbf{A}}.$$

The identity tensor is denoted by $\mathbf{1}$. The notation $\mathbf{A}^{\text{D}}$ stands for a deviatoric part of a tensor $\mathbf{A}^{\text{D}} := \mathbf{A} - \frac{1}{3}\text{tr}(\mathbf{A})\mathbf{1}$.

2. Rheological analogy

2.1. Two-dimensional rheological model

Rheological models are useful for insight into the aspects of material modeling. Especially large body of information is provided by rheological models if they are filled with a physical content (Petrov , 1998). Obviously, the conventional 1-dimensional rheological models are not suitable for the description of the yield surface distortion. Therefore, all considerations of this section are carried out in two-dimensional space $\mathbb{R}^2$. In the paper by Shutov et al. (2011), a two-dimensional rheological model was suggested, which implies that the yield surface is given by the limaçon of Pascal. *A new extended rheological model* of distortional hardening will be presented in this section.

In analogy to Shutov et al. (2011), we consider a mechanical system which consists of a tank filled with a viscous fluid, a heavy solid which rests on the flat bottom (modified St.-Venant element $m.StV$), three elastic springs (Hooke-bodies H_{ext}, H_{kin}, and H_{dis}) connected to the modified St.-Venant element, and two spheres (modified Newton elements $m.N_{\text{kin}}$ and $m.N_{\text{dis}}$)

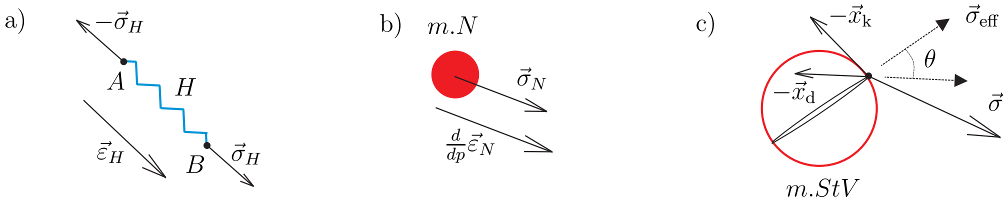

Figure 2: Behavior of idealized two-dimensional bodies: a) Hooke-body H. Its elongation is given by $\vec{\varepsilon}_H = \overrightarrow{AB} \in \mathbb{R}^2$; b) Modified Newton-body $m.N$. Inelastic arc-length p is used instead of the physical time t to formulate the constitutive equations; c) Modified St.-Venant element $m.StV$. The friction depends on the angle θ.

floating on the surface of the fluid (Fig. 1).[5] The mechanical properties of these idealized bodies are postulated as follows:

- (H): For the Hooke-bodies (see Fig. 2a), the spring force $\vec{\sigma}_H$ is proportional to the length of the body, and the force is oriented along the spring axis: $\vec{\sigma}_H = c\,\vec{\varepsilon}_H$. Here, $\vec{\varepsilon}_H = \overrightarrow{AB} \in \mathbb{R}^2$, and $c \geq 0$ is the stiffness of the spring. In particular, the Hooke-body possesses a zero length in unloaded state.

- $(m.N)$: The two-dimensional Newton element is represented by a sphere which is floating on the surface. Following the Newton's law of viscous flow, we assume that the fluid resistance $\vec{\sigma}_N$ to the motion of the sphere is proportional to its velocity $\frac{d}{dt}\vec{\varepsilon}_N$. Thus, $\frac{d}{dt}\vec{\varepsilon}_N = \varkappa\,\vec{\sigma}_N$, where $\varkappa \geq 0$ is a viscosity parameter. Next, in order to obtain the constitutive relations of the modified Newton-element, the physical time t is formally replaced by the accumulated inelastic arc-length (Odqvist parameter) p. Thus, we postulate for $(m.N)$-element (see Fig. 2b):

  $$\frac{d}{dp}\vec{\varepsilon}_N = \varkappa\,\vec{\sigma}_N. \tag{1}$$

  Such modification is possible whenever the inelastic arc-length p is available. The arc-length p will be introduced formally in the following. The use of this parameter instead of the time t allows to construct rate-independent constitutive relations (see, for example, Haupt (2002)).

---

[5] An animated version of the rheological model with only one modified Newton element is available at http://www.youtube.com/watch?v=QEPc3pixbC0

- $(m.StV)$: The heavy solid rests upon the bottom of the tank and there is a friction between them. By $\vec{\sigma}$, $-\vec{x}_{\mathrm{k}}$, and $-\vec{x}_{\mathrm{d}}$ denote now the forces acting on the $(m.StV)$-element due to the elongation of the Hooke-bodies H_{ext}, H_{kin}, and H_{dis}, respectively (see Fig. 2c). The force $\vec{\sigma}$ will be understood as an external load; $\vec{x}_{\mathrm{k}}$ and $\vec{x}_{\mathrm{d}}$ will be responsible for the effects similar to kinematic and distortional hardening, respectively. The resulting (effective) force is thus given by $\vec{\sigma}_{\mathrm{eff}} = \vec{\sigma} - \vec{x}_{\mathrm{k}} - \vec{x}_{\mathrm{d}}$. Let the axis of the $(m.StV)$-element be always oriented along the resulting (effective) force $\vec{\sigma}_{\mathrm{eff}}$. We suppose that the fluid resistance opposed the rotation of the solid is negligible. The $(m.StV)$-element remains at rest as long as $\|\vec{\sigma}_{\mathrm{eff}}\| \leq \sqrt{2/3}K$, where $\sqrt{2/3}K > 0$ is a *nonconstant* friction. The function K is computed as follows. For $\vec{x}_{\mathrm{d}} = \vec{0}$, we put $K = K_0$, where K_0 is a given basic friction. Further, suppose that $\vec{x}_{\mathrm{d}} \neq \vec{0}$. Let θ be the angle between the axis and $\vec{x}_{\mathrm{d}}$: $\theta = \arccos\Big(\frac{\vec{\sigma}_{\mathrm{eff}} \cdot \vec{x}_{\mathrm{d}}}{\|\vec{\sigma}_{\mathrm{eff}}\| \, \|\vec{x}_{\mathrm{d}}\|}\Big)$. Moreover, let $\alpha = \|\vec{x}_{\mathrm{d}}\| / x_d^{\max}$ be a distortion parameter, which is a unique function of $\|\vec{x}_{\mathrm{d}}\|$. Here, $x_d^{\max} > 0$ is the upper bound for $\|\vec{x}_{\mathrm{d}}\|$, therefore we get $\alpha \in [0,1]$. Finally, we consider the friction to be a function of θ and α: $K = \bar{K}(\theta, \alpha)\ K_0$. In particular, for a fixed $\vec{x}_{\mathrm{d}} \neq \vec{0}$, the friction K depends solely on the angle θ. A simple ansatz for $\bar{K}(\theta,\alpha)$ will be presented in the next subsection.

Remark 1. The choice of notations in this section is dictated by the need to keep the structure of the rheological model similar to the structure of small strain plasticity. For that reason, the forces imposed on the $(m.StV)$-element by the Hooke-bodies are denoted by $-\vec{x}_{\mathrm{k}}$, $-\vec{x}_{\mathrm{d}}$ rather than $\vec{x}_{\mathrm{k}}$, $\vec{x}_{\mathrm{d}}$.

2.2. Direction-dependent friction and definition of overstress

Let $\vec{e}_1 = (1,0) \in \mathbb{R}^2$. In this subsection we construct the non-dimensional function $\bar{K}(\theta,\alpha)$ which plays a central role in the current study. In terms of the rheological model introduced above, this function is understood as a friction coefficient, but in the following sections it will be treated as a non-dimensional yield stress. It is useful to interpret such functions geometrically in terms of a parametric family of closed subsets in $\mathbb{R}^2$: For each $\alpha \in [0,1]$ the corresponding subset $\mathrm{El}(\bar{K}(\cdot,\alpha))$ consists of $\vec{y} \in \mathbb{R}^2$ such that $\|\vec{y}\| \leq \bar{K}(\theta,\alpha)$, where $\theta \in [0,\pi]$ is the angle between $\vec{y}$ and $\vec{e}_1$ (cf. Fig. 3b). More precisely, we put

$$\mathrm{El}(\bar{K}(\cdot,\alpha)) := \big\{\vec{y} \in \mathbb{R}^2/\{\vec{0}\}\ :\ \|\vec{y}\| \leq \bar{K}(\theta,\alpha),\ \text{where } \theta = \widehat{(\vec{y},\vec{e}_1)}\big\} \cup \{\vec{0}\}, \quad (2)$$

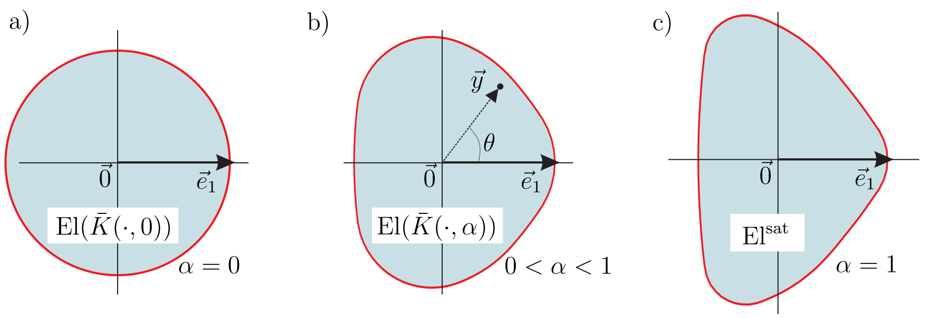

Figure 3: a) A closed unit disc which is used to represent the undistorted yield surface; b) Geometric interpretation of $\bar{K}(\theta,\alpha)$ for a fixed α. For each α a closed set $\mathrm{El}(\bar{K}(\cdot,\alpha)) \subset \mathbb{R}^2$ is defined; c) A convex set $\mathrm{El}^{\mathrm{sat}}$ corresponds to the given function $\bar{K}^{\mathrm{sat}}(\theta)$. The boundary of $\mathrm{El}^{\mathrm{sat}}$ can be associated with a saturated form of the yield surface.

$$\widehat{(\vec{y},\vec{e}_1)} := \arccos\Big(\frac{\vec{y}\cdot\vec{e}_1}{\|\vec{y}\|\ \|\vec{e}_1\|}\Big).$$

First, for $\alpha = 0$, we postulate that $\bar{K}(\theta,0) = 1$, which implies that $\mathrm{El}(\bar{K}(\cdot,0))$ is a closed unit disc in $\mathbb{R}^2$ (see Fig. 3a). Further, suppose that a smooth function $\bar{K}^{\mathrm{sat}}(\theta)$ is given such that $\mathrm{El}^{\mathrm{sat}} := \mathrm{El}(\bar{K}^{\mathrm{sat}}(\cdot))$ is convex and $\bar{K}^{\mathrm{sat}}(0) = 1$ (see Fig. 3c). We need to find a smooth function $\bar{K}(\theta,\alpha)$ such that $\mathrm{El}(\bar{K}(\cdot,\alpha))$ will be convex for all α and

$$\bar{K}(0,\alpha) = 1 \text{ for } \alpha \in [0,1], \quad \bar{K}(\theta,1) = \bar{K}^{\mathrm{sat}}(\theta) \text{ for } \theta \in [0,\pi].$$

Remark 2. As it will be shown in the following, the given function $\bar{K}^{\mathrm{sat}}(\theta)$ corresponds to the form of a saturated distortional hardening with the maximum distortion (Fig. 3c).

Remark 3. The parameter α should be understood as a distortion parameter, such that $\alpha = 0$ and $\alpha = 1$ correspond to zero and maximum distortion, respectively.

In other words, an interpolation rule is needed between the intact initial unit disc (corresponds to $\alpha = 0$) and the maximum distorted set $\mathrm{El}^{\mathrm{sat}}$ (corresponds to $\alpha = 1$).

Remark 4. Unfortunately, the linear interpolation rule $\bar{K}(\theta,\alpha) = (1-\alpha) + \alpha\bar{K}^{\mathrm{sat}}(\theta)$ is not suitable, since, in general, the convexity of $\mathrm{El}(\bar{K}(\cdot,\alpha))$ is violated for some $\alpha \in (0,1)$.

The interpolation rule which is implemented in the current study is constructed as follows. First, for any $\vec{y} \in \mathbb{R}^2$, $A \subset \mathbb{R}^2$ we define the distance in

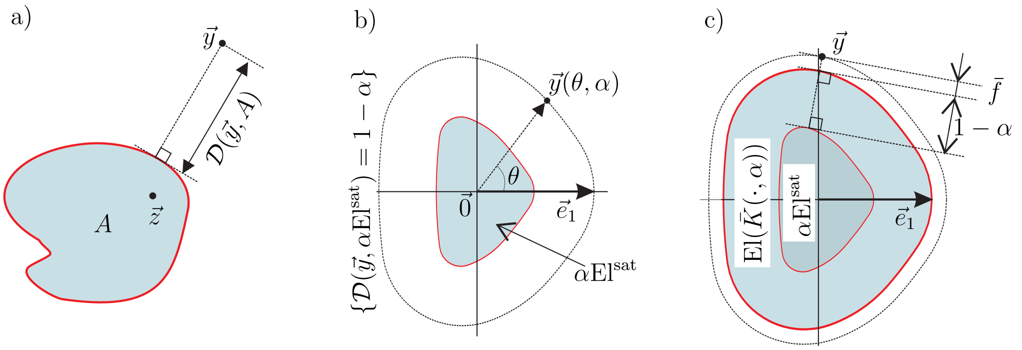
a)
$\vec{y}$
$\mathcal{D}(\vec{y},A)$
$\vec{z}$
A
b)
$\{\mathcal{D}(\vec{y},\alpha\mathrm{El}^{\mathrm{sat}})=1-\alpha\}$
$\vec{y}(\theta,\alpha)$
θ
$\vec{0}$
$\vec{e}_1$
$\alpha\mathrm{El}^{\mathrm{sat}}$
c)
$\vec{y}$
$\bar{f}$
$1-\alpha$
$\mathrm{El}(\bar{K}(\cdot,\alpha))$
$\alpha\mathrm{El}^{\mathrm{sat}}$
$\vec{e}_1$

Figure 4: a) Definition of the distance $\mathcal{D}(\vec{y},A)$ according to (3); b) Definition of $\vec{y}(\theta,\alpha)$ for $\theta\in[0,\pi]$, $\alpha\in[0,1]$; c) A line of constant overstress $\bar{f}$ for a fixed $\alpha\in[0,1]$.

a natural way (see Fig. 4a)

$$\mathcal{D}(\vec{y},A):=\inf_{\vec{z}\in A}\|\vec{y}-\vec{z}\|. \tag{3}$$

Next, we define the product of $\alpha\in\mathbb{R}$ and $A\subset\mathbb{R}^2$ as $\alpha A:=\{\alpha\vec{y}\ :\ \vec{y}\in A\}$. The set $\mathrm{El}(\bar{K}(\cdot,\alpha))$ is obtained from the set $\alpha\mathrm{El}^{\mathrm{sat}}$ by adding additional points whose distance from $\alpha\mathrm{El}^{\mathrm{sat}}$ does not exceed $1-\alpha$ (see Fig. 4b)

$$\mathrm{El}(\bar{K}(\cdot,\alpha)):=\big\{\vec{y}\in\mathbb{R}^2:\mathcal{D}(\vec{y},\alpha\mathrm{El}^{\mathrm{sat}})\leq 1-\alpha\big\}. \tag{4}$$

Since $\mathrm{El}^{\mathrm{sat}}$ is convex, so is $\mathrm{El}(\bar{K}(\cdot,\alpha))$.

Formally, since $\mathrm{El}^{\mathrm{sat}}$ is convex, for each $\theta\in[0,\pi]$, and $\alpha\in[0,1]$ there exists a unique $\vec{y}(\theta,\alpha)$ such that $\vec{y}=\|\vec{y}\|(\cos(\theta),\sin(\theta))$ and $\mathcal{D}(\vec{y},\alpha\mathrm{El}^{\mathrm{sat}})=1-\alpha$ (see Fig. 4b). Thus, in accordance with (4), we put

$$\bar{K}(\theta,\alpha):=\|\vec{y}(\theta,\alpha)\|. \tag{5}$$

In what follows, each set $\mathrm{El}(\bar{K}(\cdot,\alpha))$ will be used to reflect the elastic region in the stress space. Since a viscoplasticity model of overstress type is to be constructed, a proper definition of the overstress will be needed. For given $\vec{y}\in\mathbb{R}^2$, $\alpha\in[0,1]$ we define a non-dimensional overstress as a distance from elastic domain:

$$\bar{f}(\vec{y},\alpha):=\mathcal{D}\Big(\vec{y},\mathrm{El}(\bar{K}(\cdot,\alpha))\Big)=\big\langle\mathcal{D}\big(\vec{y},\alpha\mathrm{El}^{\mathrm{sat}}\big)-(1-\alpha)\big\rangle, \tag{6}$$

where $\langle x\rangle:=\max(x,0)$. The definition is summarized in Fig. 4c. Thus, for the numerical computation of the overstress it is sufficient to evaluate

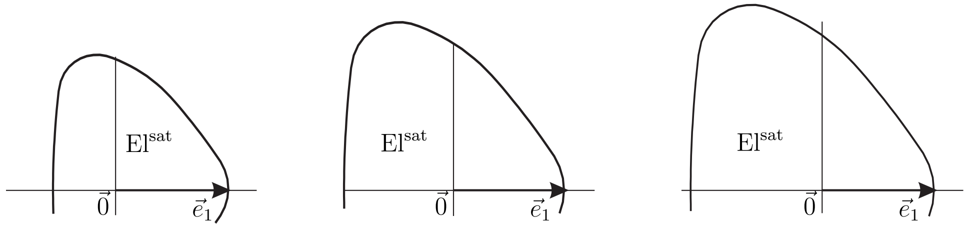

$\bar{K}^{\text{sat}}(\pi) < 1 = \bar{K}^{\text{sat}}(0)$ $\bar{K}^{\text{sat}}(\pi) = 1 = \bar{K}^{\text{sat}}(0)$ $\bar{K}^{\text{sat}}(\pi) > 1 = \bar{K}^{\text{sat}}(0)$

Figure 5: The material function $\bar{K}^{\text{sat}}(\theta)$ is not uniquely determined by the form of the saturated yield surface. The function is unique if $\bar{K}^{\text{sat}}(\pi) > 0$ is additionally specified.

$\mathcal{D}\big(\vec{y}, \alpha \text{El}^{\text{sat}}\big)$. Such computation can be performed explicitly if the boundary of El$^{\text{sat}}$ is represented by a set of circular arcs. A concrete algorithm is presented in Appendix A. Note that such requirement is not restrictive, since *any smooth convex curve* can be approximated by circular arcs with sufficient accuracy. In most cases 4 or 5 arcs are sufficient for practical purposes.

Remark 5. The definition (6) of the overstress $\bar{f}$ will be advantageous in connection with a normality flow rule. In particular, the derivative of the overstress with respect to $\vec{y}$ possesses a unit norm for $\bar{f} > 0$, i.e., $\|\frac{\partial \bar{f}(\vec{y},\alpha)}{\partial \vec{y}}\| = 1$. Moreover, the set $\{\vec{y} \ : \ \bar{f}(\vec{y}) \leq \bar{f}_0\}$ is convex for all $\bar{f}_0 \geq 0$.

Remark 6. Using the interpolation rule proposed above, the function $\bar{K}(\theta, \alpha)$ is uniquely defined by the material function $\bar{K}^{\text{sat}}(\theta)$. Here, the function $\bar{K}^{\text{sat}}(\theta)$ describes the saturated form of the convex symmetric yield surface. In some cases this form can be identified experimentally (cf. Remark 9). Figure 5 demonstrates that the function $\bar{K}^{\text{sat}}(\theta)$ is not uniquely determined even if the form of the saturated yield surface is known. This is due to the fact the the position of the origin $\vec{0}$ relative to El$^{\text{sat}}$ is not unique. The function $\bar{K}^{\text{sat}}(\theta)$ is uniquely determined by specifying $\bar{K}^{\text{sat}}(\pi) > 0$, which is a material parameter "hidden" in the material function $\bar{K}^{\text{sat}}(\theta)$. This parameter should be chosen in such a way that a better description of the experimental data is achieved.

2.3. Some constitutive equations in two-dimensions

Consider a system of (constitutive) equations as follows. The total displacement of the point A in Fig. 1 with respect to the bottom will be denoted by $\vec{\varepsilon}$. This displacement is a sum of the elastic elongation of the (H_{ext})-body and the inelastic displacement of the $(m.StV)$-body, denoted by $\vec{\varepsilon}_{\text{e}}$ and $\vec{\varepsilon}_{\text{i}}$, respectively:

$$\vec{\varepsilon} = \vec{\varepsilon}_{\mathrm{e}} + \vec{\varepsilon}_{\mathrm{i}}. \tag{7}$$

The displacement of the $(m.StV)$-body, in turn, is composed of the elastic (H_{kin})-elongation and the inelastic $(m.N_{\mathrm{kin}})$-displacement. Analogous decomposition holds for H_{dis} and $m.N_{\mathrm{dis}}$, as well:

$$\vec{\varepsilon}_{\mathrm{i}} = \vec{\varepsilon}_{\mathrm{ke}} + \vec{\varepsilon}_{\mathrm{ki}}, \quad \vec{\varepsilon}_{\mathrm{i}} = \vec{\varepsilon}_{\mathrm{de}} + \vec{\varepsilon}_{\mathrm{di}}. \tag{8}$$

The total potential energy of the system equals

$$\psi = \psi_{\mathrm{el}}(\vec{\varepsilon}_{\mathrm{e}}) + \psi_{\mathrm{kin}}(\vec{\varepsilon}_{\mathrm{ke}}) + \psi_{\mathrm{dis}}(\vec{\varepsilon}_{\mathrm{de}}) = \mu\ \|\vec{\varepsilon}_{\mathrm{e}}\|^2 + \frac{c_{\mathrm{k}}}{2}\ \|\vec{\varepsilon}_{\mathrm{ke}}\|^2 + \frac{c_{\mathrm{d}}}{2}\ \|\vec{\varepsilon}_{\mathrm{de}}\|^2.$$

Here, $\mu, c_{\mathrm{k}}, c_{\mathrm{d}} \geq 0$ are the stiffnesses of H_{ext}, H_{kin}, and H_{dis}, respectively. For the forces $\vec{\sigma}$, $\vec{x}_{\mathrm{k}}$, and $\vec{x}_{\mathrm{d}}$ we get

$$\vec{\sigma} = \frac{\partial \psi_{\mathrm{el}}(\vec{\varepsilon}_{\mathrm{e}})}{\partial \vec{\varepsilon}_{\mathrm{e}}}, \quad \vec{x}_{\mathrm{k}} = \frac{\partial \psi_{\mathrm{kin}}(\vec{\varepsilon}_{\mathrm{ke}})}{\partial \vec{\varepsilon}_{\mathrm{ke}}}, \quad \vec{x}_{\mathrm{d}} = \frac{\partial \psi_{\mathrm{dis}}(\vec{\varepsilon}_{\mathrm{de}})}{\partial \vec{\varepsilon}_{\mathrm{de}}}. \tag{9}$$

The overstress f is defined as a function of $\|\vec{\sigma}_{\mathrm{eff}}\| = \|\vec{\sigma} - \vec{x}_{\mathrm{k}} - \vec{x}_{\mathrm{d}}\|$, $\theta = \arccos\Big(\frac{\vec{\sigma}_{\mathrm{eff}}\ \cdot\ \vec{x}_{\mathrm{d}}}{\|\vec{\sigma}_{\mathrm{eff}}\|\ \|\vec{x}_{\mathrm{d}}\|}\Big)$, and the distortion parameter $\alpha = \|\vec{x}_{\mathrm{d}}\|/x_d^{\max}$ by

$$f(\vec{\sigma}, \vec{x}_{\mathrm{k}}, \vec{x}_{\mathrm{d}}) = \tilde{f}(\|\vec{\sigma}_{\mathrm{eff}}\|, \theta, \alpha) := \sqrt{\frac{2}{3}} K_0\ \bar{f}(\vec{y}, \alpha), \tag{10}$$

$$\vec{y} := \frac{\|\vec{\sigma}_{\mathrm{eff}}\|}{\sqrt{2/3} K_0} (\cos(\theta), \sin(\theta)). \tag{11}$$

Due to the fact that $\|\frac{\partial \bar{f}(\vec{y},\alpha)}{\partial \vec{y}}\| = 1$ for positive overstress, we have

$$\Big\| \frac{\partial f(\vec{\sigma}, \vec{x}_{\mathrm{k}}, \vec{x}_{\mathrm{d}})}{\partial \vec{\sigma}} \Big\| = 1, \text{ for } f > 0.$$

We postulate the normality flow rule (normality to the hypersurface of constant overstress) in combination with the Perzyna-type of viscoplasticity (Perzyna , 1963)

$$\dot{\vec{\varepsilon}}_{\mathrm{i}} = \lambda_{\mathrm{i}} \frac{\partial f(\vec{\sigma}, \vec{x}_{\mathrm{k}}, \vec{x}_{\mathrm{d}})}{\partial \vec{\sigma}}, \text{ for } f > 0, \quad \dot{\vec{\varepsilon}}_{\mathrm{i}} = \vec{0} \text{ for } f = 0; \quad \lambda_{\mathrm{i}} = \frac{1}{\eta}\Big(\frac{1}{k_0} f\Big)^m.$$

Here, $\eta > 0$ and $m \geq 1$ are parameters of the Perzyna rule; $k_0 > 0$ is used to get a dimensionless term in the parentheses.

Note that the forces $\vec{x}_{\mathrm{k}}$ and $\vec{x}_{\mathrm{d}}$ act on the modified Newton-elements $m.N_{\mathrm{kin}}$ and $m.N_{\mathrm{dis}}$, respectively. Thus, we get in accordance with (1)

$$\frac{d\,\vec{\varepsilon}_{\mathrm{ki}}}{dp} = \varkappa_{\mathrm{k}}\ \vec{x}_{\mathrm{k}}, \quad \frac{d\,\vec{\varepsilon}_{\mathrm{di}}}{dp} = \varkappa_{\mathrm{d}}\ \vec{x}_{\mathrm{d}}.$$

Here, $\varkappa_{\mathrm{k}}, \varkappa_{\mathrm{d}} \geq 0$ are modified viscosity parameters describing $m.N_{\mathrm{kin}}$ and $m.N_{\mathrm{dis}}$, respectively. Let the evolution of the inelastic arc-length p be given by $\dot{p} = \lambda_{\mathrm{i}} = \|\dot{\vec{\varepsilon}}_{\mathrm{i}}\|$. Thus, we obtain

$$\dot{\vec{\varepsilon}}_{\mathrm{ki}} = \lambda_{\mathrm{i}}\ \varkappa_{\mathrm{k}}\ \vec{x}_{\mathrm{k}}, \quad \dot{\vec{\varepsilon}}_{\mathrm{di}} = \lambda_{\mathrm{i}}\ \varkappa_{\mathrm{d}}\ \vec{x}_{\mathrm{d}}. \tag{12}$$

It follows from $(9)_3$ and $(12)_2$ that for proper initial conditions we have $\|\vec{x}_{\mathrm{d}}\| \leq 1/\varkappa_{\mathrm{d}}$. By putting $x_d^{\max} = 1/\varkappa_{\mathrm{d}}$ we specify the definition of the distortion parameter α (cf. Section 2.1)

$$\alpha := \varkappa_{\mathrm{d}}\ \|\vec{x}_{\mathrm{d}}\|. \tag{13}$$

Equations (12) in combination with $(9)_2$ and $(9)_3$ describe the evolution of the "backstresses" in the hardening/recovery format. The saturation of $\vec{x}_{\mathrm{d}}$ implies the saturation of the "distortional hardening", which takes place much faster than the saturation of the "kinematic hardening". Thus, "slow" and "fast" saturation should be assumed for $\vec{x}_{\mathrm{k}}$ and $\vec{x}_{\mathrm{d}}$, respectively. Note that the dependence on the strain path is captured in a vivid way, such that the system exhibits fading memory: only the most recent part of the $\vec{\varepsilon}$-path influences the current "stress" state $\vec{\sigma}$.

3. Material model of viscoplasticity

3.1. Closed system of constitutive equations

Let us formulate a system of constitutive equations of viscoplasticity. First, we suppose that the volumetric response is elastic. More precisely, the hydrostatic stress component $\mathrm{tr}\boldsymbol{\sigma}$ is assumed to be a linear function of $\mathrm{tr}\boldsymbol{\varepsilon}$. Next, suppose that the deviatoric stress component $\boldsymbol{\sigma}^{\mathrm{D}}$ depends solely on the history of the strain deviator $\boldsymbol{\varepsilon}^{\mathrm{D}}$. In order to describe this dependence, we generalize the two-dimensional constitutive equations presented in the previous section to five dimensions.[6] During the generalization we have to make sure that the resulting model inherits the properties of the two-dimensional rheological model. Toward that end, the displacements and forces are formally replaced by deviatoric strains and stresses, respectively; the scalar product in $\mathbb{R}^2$ is replaced by the scalar product of two second-rank tensors.[7] In order to take the isotropic hardening into account, the constant parameter K_0 is now formally replaced by $K_0 + R$, where R is a hardening variable. In order to describe the evolution of R, we introduce a scalar strain-like internal variable s (which is similar to the inelastic arc-length p), its dissipative part s_{d}, and its conservative part s_{e}.

---

[6] Mathematically, $\boldsymbol{\sigma}^{\mathrm{D}}$ and $\boldsymbol{\varepsilon}^{\mathrm{D}}$ are elements of a 5-dimensional vector space of trace-free (deviatoric) second rank symmetric tensors.

For the strain tensor $\boldsymbol{\varepsilon}$ consider its inelastic part $\boldsymbol{\varepsilon}_{\text{i}}$ and elastic part $\boldsymbol{\varepsilon}_{\text{e}}$. Let $\boldsymbol{\varepsilon}_{\text{ki}}$ and $\boldsymbol{\varepsilon}_{\text{ke}}$ be the dissipative and conservative parts of $\boldsymbol{\varepsilon}_{\text{i}}$, which are connected to the nonlinear kinematic hardening. Analogously, $\boldsymbol{\varepsilon}_{\text{di}}$ and $\boldsymbol{\varepsilon}_{\text{de}}$ are parts of $\boldsymbol{\varepsilon}_{\text{i}}$ associated to the distortional hardening. More precisely, we postulate

$$\boldsymbol{\varepsilon} = \boldsymbol{\varepsilon}_{\text{e}} + \boldsymbol{\varepsilon}_{\text{i}}, \quad \boldsymbol{\varepsilon}_{\text{i}} = \boldsymbol{\varepsilon}_{\text{ke}} + \boldsymbol{\varepsilon}_{\text{ki}}, \quad \boldsymbol{\varepsilon}_{\text{i}} = \boldsymbol{\varepsilon}_{\text{de}} + \boldsymbol{\varepsilon}_{\text{di}}, \quad s = s_{\text{e}} + s_{\text{d}}. \tag{14}$$

Note that the first decomposition is related to (7). Moreover, $(14)_2$ and $(14)_3$ can be motivated by (8). The evolution of the state of the material is captured by the inelastic flow $\dot{\boldsymbol{\varepsilon}}_{\text{i}}$ and the inelastic flow $(\dot{\boldsymbol{\varepsilon}}_{\text{ki}}, \dot{\boldsymbol{\varepsilon}}_{\text{di}}, \dot{s}_{\text{d}})$ which takes place on the microstructural level.

The specific free energy per unit mass is given by

$$\psi = \psi_{\text{el}}(\boldsymbol{\varepsilon}_{\text{e}}) + \psi_{\text{kin}}(\boldsymbol{\varepsilon}_{\text{ke}}) + \psi_{\text{dis}}(\boldsymbol{\varepsilon}_{\text{de}}) + \psi_{\text{iso}}(s_{\text{e}}), \tag{15}$$

$$\rho\psi_{\text{el}}(\boldsymbol{\varepsilon}_{\text{e}}) = \frac{k}{2}(\text{tr } \boldsymbol{\varepsilon}_{\text{e}})^2 + \mu \, \|\boldsymbol{\varepsilon}_{\text{e}}^{\text{D}}\|^2, \quad \rho\psi_{\text{kin}}(\boldsymbol{\varepsilon}_{\text{ke}}) = \frac{c_{\text{k}}}{2} \, \|\boldsymbol{\varepsilon}_{\text{ke}}^{\text{D}}\|^2, \tag{16}$$

$$\rho\psi_{\text{dis}}(\boldsymbol{\varepsilon}_{\text{de}}) = \frac{c_{\text{d}}}{2} \, \|\boldsymbol{\varepsilon}_{\text{de}}^{\text{D}}\|^2, \quad \rho\psi_{\text{iso}}(s_{\text{e}}) = \frac{\gamma}{2}(s_{\text{e}})^2. \tag{17}$$

Here, $k, \mu, c_{\text{k}}, c_{\text{d}}, \gamma \geq 0$ are material parameters; $\rho > 0$ stands for the mass density. The quantity $\psi_{\text{el}}(\boldsymbol{\varepsilon}_{\text{e}})$ stands for the energy stored due to macroscopic elastic deformations. The remaining part $\psi_{\text{kin}} + \psi_{\text{dis}} + \psi_{\text{iso}}$ is used to capture the energy associated with the defects of the crystal structure.[8] Next, we postulate the following relations for stresses, backstresses, and isotropic hardening

---

[7] Using a similar approach, a two-dimensional rheological model was already generalized to cover *finite strain* vsicoplasticity (Shutov et al. , 2011).

[8] Note that $\psi_{\text{kin}} + \psi_{\text{dis}} + \psi_{\text{iso}}$ does not necessarily reflect the entire "defect energy". It is natural to assume that a part of the "defect energy" is not connected to any hardening

$$\boldsymbol{\sigma} = \rho \frac{\partial \psi_{\mathrm{el}}(\boldsymbol{\varepsilon}_{\mathrm{e}})}{\partial \boldsymbol{\varepsilon}_{\mathrm{e}}}, \ \boldsymbol{X}_{\mathrm{k}} = \rho \frac{\partial \psi_{\mathrm{kin}}(\boldsymbol{\varepsilon}_{\mathrm{ke}})}{\partial \boldsymbol{\varepsilon}_{\mathrm{ke}}}, \ \boldsymbol{X}_{\mathrm{d}} = \rho \frac{\partial \psi_{\mathrm{dis}}(\boldsymbol{\varepsilon}_{\mathrm{de}})}{\partial \boldsymbol{\varepsilon}_{\mathrm{de}}}, \ R = \rho \frac{\partial \psi_{\mathrm{iso}}(s_{\mathrm{e}})}{\partial s_{\mathrm{e}}}. \tag{18}$$

Substituting (16) and (17) into (18) we get

$$\boldsymbol{\sigma} = k \ \mathrm{tr}(\boldsymbol{\varepsilon}_{\mathrm{e}})\mathbf{1} + 2\mu \boldsymbol{\varepsilon}_{\mathrm{e}}^{\mathrm{D}}, \ \boldsymbol{X}_{\mathrm{k}} = c_{\mathrm{k}} \boldsymbol{\varepsilon}_{\mathrm{ke}}^{\mathrm{D}}, \ \boldsymbol{X}_{\mathrm{d}} = c_{\mathrm{d}} \boldsymbol{\varepsilon}_{\mathrm{de}}^{\mathrm{D}}, \ R = \gamma s_{\mathrm{e}}. \tag{19}$$

On the one hand, these relations can be motivated by the rheological model from Section 2. On the other hand, as it will be shown in the following, relations (18) will be sufficient for the thermodynamic consistency of the material model. It follows immediately from (19) that $\mathrm{tr}\boldsymbol{X}_{\mathrm{k}} = \mathrm{tr}\boldsymbol{X}_{\mathrm{d}} = 0$.

Suppose that the degree of distortion α depends solely on $\|\boldsymbol{X}_{\mathrm{d}}\|$. A concrete dependence will be specified in the following (cf. (26)). The effective stress tensor and the angle θ are defined now through

$$\boldsymbol{\sigma}_{\mathrm{eff}} := \boldsymbol{\sigma} - \boldsymbol{X}_{\mathrm{k}} - \boldsymbol{X}_{\mathrm{d}}, \quad \theta := \arccos\Big(\frac{\boldsymbol{\sigma}_{\mathrm{eff}}^{\mathrm{D}} : \boldsymbol{X}_{\mathrm{d}}}{\|\boldsymbol{\sigma}_{\mathrm{eff}}^{\mathrm{D}}\| \ \|\boldsymbol{X}_{\mathrm{d}}\|} \Big). \tag{20}$$

Note that for $\|\boldsymbol{X}_{\mathrm{d}}\| = 0$ the angle θ is arbitrary. To be definite, we put $\theta = 0$ in that case. Further, analogously to (10) and (11), we define $\vec{y} \in \mathbb{R}^2$ and the corresponding overstress f (see Fig. 6a)

$$f(\boldsymbol{\sigma}, \boldsymbol{X}_{\mathrm{k}}, \boldsymbol{X}_{\mathrm{d}}, R) = \tilde{f}(\|\boldsymbol{\sigma}_{\mathrm{eff}}^{\mathrm{D}}\|, \theta, \alpha, R) := \sqrt{\frac{2}{3}}(K_0 + R) \ \bar{f}(\vec{y}, \alpha), \tag{21}$$

$$\vec{y} := \frac{\|\boldsymbol{\sigma}_{\mathrm{eff}}^{\mathrm{D}}\|}{\sqrt{2/3}(K_0 + R)} (\cos(\theta), \sin(\theta)). \tag{22}$$

Here, $K_0 > 0$ is a fixed material parameter (initial yield stress), and the function $\bar{f}(\vec{y}, \alpha)$ is defined through (6).

---

mechanism (Shutov and Ihlemann , 2011). Alternatively, Henann and Anand (2009) prefer to neglect the free energy storage ψ_{iso} which is associated with the isotropic hardening. Interestingly, Feigenbaum and Dafalias (2008) suggest that the defect energy is released while the distortion of the yield surface takes place. Thus, again, somewhat smaller energy storage will be predicted than by assumption (15). The choice between many alternatives is important for the prediction of the inelastic dissipation and should be based on relevant experimental observations.

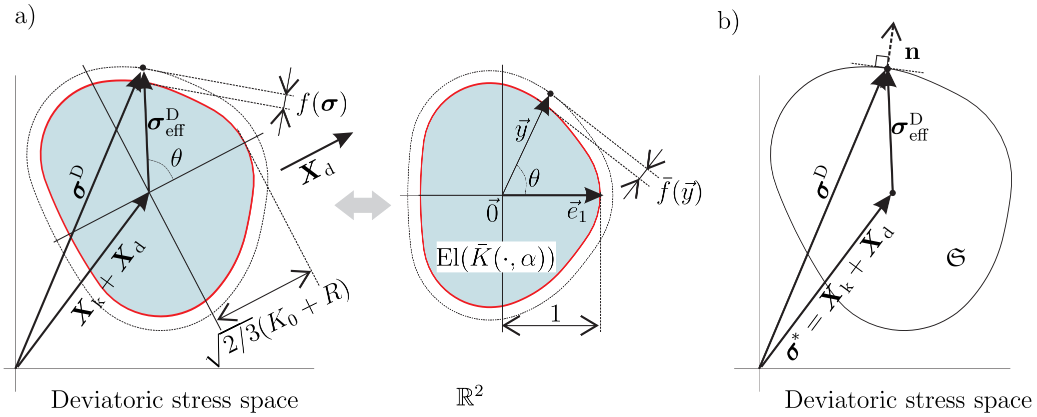
a)
b)
$f(\boldsymbol{\sigma})$
$\boldsymbol{\sigma}^{\mathrm{D}}_{\mathrm{eff}}$
θ
$\boldsymbol{X}_{\mathrm{d}}$
$\boldsymbol{\sigma}^{D}$
$\boldsymbol{X}_{\mathrm{k}} + \boldsymbol{X}_{\mathrm{d}}$
$\sqrt{2/3}(K_0 + R)$
$\vec{y}$
$\vec{0}$
$\vec{e}_1$
$\bar{f}(\vec{y})$
$\mathrm{El}(\bar{K}(\cdot, \alpha))$
1
$\mathbf{n}$
$\boldsymbol{\sigma}^{*} = \boldsymbol{X}_{\mathrm{k}} + \boldsymbol{X}_{\mathrm{d}}$
$\mathfrak{S}$
Deviatoric stress space
$\mathbb{R}^2$
Deviatoric stress space

Figure 6: a) Sketch of the yield surface in the deviatoric stress space and definition of the overstress $f(\boldsymbol{\sigma})$ (cf. (20), (21)). The elastic domain in the stress space is associated with $\mathrm{El}(\bar{K}(\cdot, \alpha)) \subset \mathbb{R}^2$; b) Sketch of the proof of the inequality (27).

The elastic domain corresponds to stress states with zero overstress f. For a given stress tensor $\boldsymbol{\sigma}$, a non-dimensional vector $\vec{y} \in \mathbb{R}^2$ must be evaluated according to (22). Observe that the angle between $\vec{y}$ and $\vec{e}_1$ coincides with the angle between $\boldsymbol{\sigma}^{\mathrm{D}}_{\mathrm{eff}}$ and $\boldsymbol{X}_{\mathrm{d}}$ (see Fig. 6a). According to (21), the stress state $\boldsymbol{\sigma}$ lies within the elastic domain if and only if $\vec{y} \in \mathrm{El}(\bar{K}(\cdot, \alpha))$. The origin of the elastic domain corresponds to $\{\vec{y} = \vec{0}\}$ or, equivalently, $\{\boldsymbol{\sigma}^{\mathrm{D}}_{\mathrm{eff}} = \mathbf{0}\} = \{\boldsymbol{\sigma}^{\mathrm{D}} = \boldsymbol{X}_{\mathrm{k}} + \boldsymbol{X}_{\mathrm{d}}\}$. Next, observe that the direction of the elastic domain coincides with the direction of $\boldsymbol{X}_{\mathrm{d}}$, and the size of the elastic domain in that direction equals $\sqrt{\frac{2}{3}}(K_0 + R)$ (see Fig. 6a).

Remark 7. The relations (21) and (22) imply that the resistance to plastic deformation depends on the actual direction of the loading relative to the recent loading path. This dependence on the loading direction can be associated with the activation/deactivation of crystallographic slip planes as well as mobilization/demobilization of oriented dislocation structures. It is well known that the gliding of dislocations is obstructed by the cell walls under monotonic loading ($\theta = 0$), but after a strain path change ($\theta \neq 0$), the loading may drive the dislocations toward the cell interior (Viatkina et al. , 2007). In the monograph by Viatkina (2005), the mechanism of “directional remobilisation” under the strain path change is explained as a remobilisation of dislocation locks and dipoles which were formed during the previous loading, in contrast to the statistical remobilisation which is independent of the strain path change.

The normality flow rule in combination with the Perzyna rule is used

$$\dot{\boldsymbol{\varepsilon}}_{\rm i} = \lambda_{\rm i} \frac{\partial f(\boldsymbol{\sigma}, \boldsymbol{X}_{\rm k}, \boldsymbol{X}_{\rm d}, R)}{\partial \boldsymbol{\sigma}} \text{ for } f > 0, \ \dot{\boldsymbol{\varepsilon}}_{\rm i} = \mathbf{0} \text{ for } f = 0; \quad \lambda_{\rm i} = \frac{1}{\eta}\Big(\frac{1}{k_0} f\Big)^m. \tag{23}$$

Here, $\lambda_{\rm i} \geq 0$ is an inelastic multiplier which controls the rate of the inelastic flow. Indeed, since $\|\frac{\partial \bar{f}(\bar{y},\alpha)}{\partial \bar{y}}\| = 1$ for $\bar{f} > 0$, we get (cf. (43))

$$\Big\| \frac{\partial f(\boldsymbol{\sigma}, \boldsymbol{X}_{\rm k}, \boldsymbol{X}_{\rm d}, R)}{\partial \boldsymbol{\sigma}} \Big\| = 1 \text{ for } f > 0, \quad \|\dot{\boldsymbol{\varepsilon}}_{\rm i}\| = \lambda_{\rm i}, \quad \dot{p} = \lambda_{\rm i}. \tag{24}$$

We emphasize that k_0 is not a material parameter, and we put $k_0 = 1$ MPa. A concrete algorithm for the evaluation of the derivative $\frac{\partial f(\boldsymbol{\sigma})}{\partial \boldsymbol{\sigma}}$ is presented in Appendix B. Note that the normality rule (23) implies an incompressible flow: $\text{tr}\dot{\boldsymbol{\varepsilon}}_{\rm i} = 0$. In order to take the saturation of the kinematic and distortional hardening into account, we postulate for the inelastic flows on the microstructural level (cf. (12))

$$\dot{\boldsymbol{\varepsilon}}_{\rm ki} = \lambda_{\rm i} \ \varkappa_{\rm k} \ \boldsymbol{X}_{\rm k}, \quad \dot{\boldsymbol{\varepsilon}}_{\rm di} = \lambda_{\rm i} \ \varkappa_{\rm d} \ \boldsymbol{X}_{\rm d}. \tag{25}$$

Here, $\varkappa_{\rm k}, \varkappa_{\rm d} \geq 0$ are material parameters. Recall that $\text{tr}\boldsymbol{X}_{\rm k} = \text{tr}\boldsymbol{X}_{\rm d} = 0$. Thus, the inelastic flow on the microstructural level is incompressible as well: $\text{tr}\dot{\boldsymbol{\varepsilon}}_{\rm ki} = \text{tr}\dot{\boldsymbol{\varepsilon}}_{\rm di} = 0$. It can be easily shown that for $\|\boldsymbol{X}_{\rm d}\||_{t=0} \leq 1/\varkappa_{\rm d}$ we have $\|\boldsymbol{X}_{\rm d}\| \leq 1/\varkappa_{\rm d}$. Thus, analogously to (13), we define the distortion parameter $\alpha \in [0, 1]$ by

$$\alpha := \varkappa_{\rm d} \ \|\boldsymbol{X}_{\rm d}\|. \tag{26}$$

For a given deviatoric stress $\boldsymbol{\sigma}^{\rm D}$ consider a convex set $\mathfrak{S} = \{\boldsymbol{\sigma}^* : \ \text{tr}\boldsymbol{\sigma}^* = 0, \quad f(\boldsymbol{\sigma}^*) \leq f(\boldsymbol{\sigma}^{\rm D})\}$. The gradient $\frac{\partial f(\boldsymbol{\sigma}, \boldsymbol{X}_{\rm k}, \boldsymbol{X}_{\rm d}, R)}{\partial \boldsymbol{\sigma}}$ coincides with the unit outward normal $\mathbf{n}$ to the boundary of $\mathfrak{S}$ at $\boldsymbol{\sigma}^{\rm D}$. Moreover, the state $\boldsymbol{\sigma}^* = \boldsymbol{X}_{\rm k} + \boldsymbol{X}_{\rm d}$ lies within $\mathfrak{S}$ (cf. Fig. 6b). Due to the convexity of $\mathfrak{S}$ we have

$$\boldsymbol{\sigma}^{\rm D}_{\rm eff} : \dot{\boldsymbol{\varepsilon}}_{\rm i} \overset{(23)}{=} \lambda_{\rm i}(\boldsymbol{\sigma}^{\rm D} - \boldsymbol{\sigma}^*) : \mathbf{n} \geq 0. \tag{27}$$

Having this inequality in mind we formulate the evolution equations for the internal variable s and its dissipative part $s_{\rm d}$:

$$\dot{s} = \frac{\boldsymbol{\sigma}_{\rm eff} : \dot{\boldsymbol{\varepsilon}}_{\rm i}}{K_0 + R} \overset{\text{tr}\dot{\boldsymbol{\varepsilon}}_{\rm i}=0}{=} \frac{\boldsymbol{\sigma}^{\rm D}_{\rm eff} : \dot{\boldsymbol{\varepsilon}}_{\rm i}}{K_0 + R}, \qquad \dot{s}_{\rm d} = \frac{\beta}{\gamma} \dot{s} R, \tag{28}$$

where $\beta \geq 0$ is a material parameter controlling the saturation of the isotropic hardening. It follows from (27) that $\dot{s} \geq 0$. Thus, similar to the inelastic arc-length, the variable s increases monotonically. Note that in the case of proportional monotonic loading we have $\theta \approx 0$. Thus, $\boldsymbol{\sigma}^{\mathrm{D}}_{\mathrm{eff}} : \dot{\boldsymbol{\varepsilon}}_{\mathrm{i}} \approx \|\boldsymbol{\sigma}^{\mathrm{D}}_{\mathrm{eff}}\| \, \|\dot{\boldsymbol{\varepsilon}}_{\mathrm{i}}\| = \|\boldsymbol{\sigma}^{\mathrm{D}}_{\mathrm{eff}}\| \, \lambda_{\mathrm{i}}$. Moreover, for slow loading we get $f \ll (K_0 + R)$. Therefore, $\|\boldsymbol{\sigma}^{\mathrm{D}}_{\mathrm{eff}}\| \approx \sqrt{2/3}\,(K_0 + R)$. Thus, under quasistatic proportional loading, the parameter s evolves similar to the inelastic arc-length: $\dot{s} \approx \sqrt{2/3}\, \|\dot{\boldsymbol{\varepsilon}}_{\mathrm{i}}\| = \sqrt{2/3}\lambda_{\mathrm{i}}$. Under general loading conditions, although, the evolution of s depends not only on the rate of the plastic flow, but also on its direction.

Finally, the system of constitutive equations is closed by initial conditions imposed on the strain-like internal variables

$$\boldsymbol{\varepsilon}_{\mathrm{i}}|_{t=0} = \boldsymbol{\varepsilon}^0_{\mathrm{i}}, \ \boldsymbol{\varepsilon}_{\mathrm{ki}}|_{t=0} = \boldsymbol{\varepsilon}^0_{\mathrm{ki}}, \ \boldsymbol{\varepsilon}_{\mathrm{di}}|_{t=0} = \boldsymbol{\varepsilon}^0_{\mathrm{di}}, \ s|_{t=0} = s^0, \ s_{\mathrm{d}}|_{t=0} = s^0_{\mathrm{d}}.$$

We suppose $\mathrm{tr}\boldsymbol{\varepsilon}^0_{\mathrm{i}} = \mathrm{tr}\boldsymbol{\varepsilon}^0_{\mathrm{ki}} = \mathrm{tr}\boldsymbol{\varepsilon}^0_{\mathrm{di}} = 0$. If the undeformed state is assumed to be stress free at $t = 0$, then $\boldsymbol{\varepsilon}^0_{\mathrm{i}} = \mathbf{0}$. The quantities $\boldsymbol{\varepsilon}^0_{\mathrm{ki}}$ and $\boldsymbol{\varepsilon}^0_{\mathrm{di}}$ can be used to capture the initial plastic anisotropy of the material.[9] In particular, the yield condition at $t = 0$ does not have to coincide with the Huber-Mises criterium.

3.2. Proof of thermodynamic consistency

Let us consider the Clausius-Duhem inequality in the form (see, for example, Haupt (2002))

$$\delta_{\mathrm{i}} := \frac{1}{\rho}\boldsymbol{\sigma} : \dot{\boldsymbol{\varepsilon}} - \dot{\psi} \geq 0. \tag{29}$$

Taking the kinematic relations (14) into account, we rewrite the stress power as follows

$$\begin{aligned} &\boldsymbol{\sigma} : \dot{\boldsymbol{\varepsilon}} = \\ &\boldsymbol{\sigma} : (\dot{\boldsymbol{\varepsilon}}_{\mathrm{e}} + \dot{\boldsymbol{\varepsilon}}_{\mathrm{i}}) - \boldsymbol{X}_{\mathrm{k}} : \dot{\boldsymbol{\varepsilon}}_{\mathrm{i}} + \boldsymbol{X}_{\mathrm{k}} : (\dot{\boldsymbol{\varepsilon}}_{\mathrm{ki}} + \dot{\boldsymbol{\varepsilon}}_{\mathrm{ke}}) - \boldsymbol{X}_{\mathrm{d}} : \dot{\boldsymbol{\varepsilon}}_{\mathrm{i}} + \boldsymbol{X}_{\mathrm{d}} : (\dot{\boldsymbol{\varepsilon}}_{\mathrm{di}} + \dot{\boldsymbol{\varepsilon}}_{\mathrm{de}}). \end{aligned} \tag{30}$$

Moreover, differentiating (15), we get for the time derivative of the free energy

$$\dot{\psi} = \frac{\partial \psi_{\mathrm{el}}(\boldsymbol{\varepsilon}_{\mathrm{e}})}{\partial \boldsymbol{\varepsilon}_{\mathrm{e}}} : \dot{\boldsymbol{\varepsilon}}_{\mathrm{e}} + \frac{\partial \psi_{\mathrm{kin}}(\boldsymbol{\varepsilon}_{\mathrm{ke}})}{\partial \boldsymbol{\varepsilon}_{\mathrm{ke}}} : \dot{\boldsymbol{\varepsilon}}_{\mathrm{ke}} + \frac{\partial \psi_{\mathrm{dis}}(\boldsymbol{\varepsilon}_{\mathrm{de}})}{\partial \boldsymbol{\varepsilon}_{\mathrm{de}}} : \dot{\boldsymbol{\varepsilon}}_{\mathrm{de}} + \frac{\partial \psi_{\mathrm{iso}}(s_{\mathrm{e}})}{\partial s_{\mathrm{e}}} \dot{s}_{\mathrm{e}}. \tag{31}$$

---

[9] This is equivalent to the introduction of initial backstresses.

Substituting (30) and (31) into (29) and taking the potential relations (18) into account, we obtain the Clausius-Duhem inequality in the following form

$$\rho\ \delta_{\mathrm{i}} = \big(\boldsymbol{\sigma}_{\mathrm{eff}} : \dot{\boldsymbol{\varepsilon}}_{\mathrm{i}} - R\ \dot{s}\big) + \boldsymbol{X}_{\mathrm{k}} : \dot{\boldsymbol{\varepsilon}}_{\mathrm{ki}} + \boldsymbol{X}_{\mathrm{d}} : \dot{\boldsymbol{\varepsilon}}_{\mathrm{di}} + R\dot{s}_{\mathrm{d}} \geq 0.$$

It follows immediately from (25) and $(28)_2$ that $\boldsymbol{X}_{\mathrm{k}} : \dot{\boldsymbol{\varepsilon}}_{\mathrm{ki}} \geq 0$, $\boldsymbol{X}_{\mathrm{d}} : \dot{\boldsymbol{\varepsilon}}_{\mathrm{di}} \geq 0$, and $R\dot{s}_{\mathrm{d}} \geq 0$. In order to prove the thermodynamic consistency of the material model it remains to show that $\boldsymbol{\sigma}_{\mathrm{eff}} : \dot{\boldsymbol{\varepsilon}}_{\mathrm{i}} - R\ \dot{s} \geq 0$. Indeed,

$$\boldsymbol{\sigma}_{\mathrm{eff}} : \dot{\boldsymbol{\varepsilon}}_{\mathrm{i}} - R\ \dot{s} \overset{(28)_1}{=} \boldsymbol{\sigma}^{\mathrm{D}}_{\mathrm{eff}} : \dot{\boldsymbol{\varepsilon}}_{\mathrm{i}}\ (1 - R/(K_0 + R)) = \boldsymbol{\sigma}^{\mathrm{D}}_{\mathrm{eff}} : \dot{\boldsymbol{\varepsilon}}_{\mathrm{i}}\ (K_0/(K_0 + R)) \overset{(27)}{\geq} 0.$$

The thermodynamic consistency of the material model is thus proved.

Remark 8. Note that the proof of the thermodynamic consistency is essentially based on the inequality $\boldsymbol{\sigma}^{\mathrm{D}}_{\mathrm{eff}} : \dot{\boldsymbol{\varepsilon}}_{\mathrm{i}} \geq 0$. *Any flow rule* which governs $\dot{\boldsymbol{\varepsilon}}_{\mathrm{i}}$ and complies with this inequality would yield a thermodynamically consistent material model, as well. For instance, the radial flow rule can be considered as a simplified alternative to the normality rule $(23)_1$

$$\dot{\boldsymbol{\varepsilon}}_{\mathrm{i}} = \lambda_{\mathrm{i}} \boldsymbol{R}_{\mathrm{eff}}, \quad \boldsymbol{R}_{\mathrm{eff}} := \frac{\boldsymbol{\sigma}^{\mathrm{D}}_{\mathrm{eff}}}{\|\boldsymbol{\sigma}^{\mathrm{D}}_{\mathrm{eff}}\|}. \tag{32}$$

3.3. Identification of material parameters

The material model contains 11 material parameters and a material function $\bar{K}^{\mathrm{sat}}(\theta)$. Let us discuss the identification of these quantities. First, the elasticity parameters k and μ can be determined basing on the experimental data for elastic deformations. Next, the initial yield stress K_0 can be calibrated using the graphical method from a quasistatic uniaxial tension test. The viscosity parameters η and m of the Perzyna law are typically identified using a series of tests under monotonic loading with different loading rates. Further, the material function $\bar{K}^{\mathrm{sat}}(\theta)$ is uniquely determined for the fixed $\bar{K}^{\mathrm{sat}}(\pi)$ if the form of the saturated yield surface is known (for details see Remark 6). For simplicity, one may assume $\bar{K}^{\mathrm{sat}}(\pi) = 1$. In that case, the parameters of isotropic hardening (γ and β) can be identified using the information about how the size of the elastic domain evolves under monotonic loading. Finally, it remains to identify two parameters of kinematic hardening (c_{k} and $\varkappa_{\mathrm{k}}$) and two distortional parameters (c_{d} and $\varkappa_{\mathrm{d}}$). This can be done by minimization of a least-squares functional which represents the discrepancy between measurements data and corresponding model predictions. Experimental measurements related to non-proportional loading are necessary in order to obtain a reliable identification procedure. Some regularization techniques can be used to reduce the correlation among the parameters and to reduce the probability of getting trapped in local minima (Shutov and Kreißig , 2010).

The success of the identification procedure depends on the quality of initial approximation chosen for the unknown parameters c_{k}, c_{d}, $\varkappa_{\mathrm{k}}$, and $\varkappa_{\mathrm{d}}$. The order of magnitude of these parameters can be estimated basing on the following considerations: The upper bounds for $\|\boldsymbol{X}_{\mathrm{k}}\|$ and $\|\boldsymbol{X}_{\mathrm{d}}\|$ are given by $\varkappa_{\mathrm{k}}^{-1}$ and $\varkappa_{\mathrm{d}}^{-1}$, respectively. At the same time, the increment of the inelastic arc-length which corresponds to the saturation of kinematic and distortional hardening under proportional loading is proportional to $(c_{\mathrm{k}}\varkappa_{\mathrm{k}})^{-1}$ and $(c_{\mathrm{d}}\varkappa_{\mathrm{d}})^{-1}$, respectively.

4. Numerical computations

In this study, for simplicity, the evolution equations (23), (25), and (28) are integrated numerically using explicit time-stepping scheme. If rate-independent material response is to be simulated, a viscous regularization with fictitious small viscosity $\eta > 0$ can be used.[10]

In this section we validate the predictive capabilities of the material model. Toward that end, we consider experimental data of Khan et al. (2010a) obtained for a very high work hardening aluminum alloy - annealed 1100 Al. The yield points were identified experimentally under combined tension-torsion of thin-walled tubular specimens using a small proof strain. In order to simulate the deformation of thin-walled tubular specimen we compute the stress response at a single material point. Consider a Cartesian coordinate system such that its basis vectors $\mathbf{e}_1$, $\mathbf{e}_2$, and $\mathbf{e}_3$ are oriented along the local axial, hoop, and radial directions, respectively. The stress state can be idealized approximately as a special case of the plane stress:

$$\boldsymbol{\sigma} = \sigma_{11}\mathbf{e}_1 \otimes \mathbf{e}_1 + \sigma_{12}(\mathbf{e}_1 \otimes \mathbf{e}_2 + \mathbf{e}_2 \otimes \mathbf{e}_1). \tag{33}$$

Here, σ_{11} and σ_{12} are associated to the axial and torsional loading, respectively. The measurement results are represented in the $(\sigma_{11}, \sqrt{3}\sigma_{12})$-space in Fig. 7a. The initial yield surface can be approximated with sufficient accuracy using the conventional Huber-Mises yield condition. Therefore, an initial plastic isotropy will be assumed during the material modeling. The yield points which were determined after 2% axial prestrain are depicted in Fig. 7a, as well. The material parameters used to simulate the material response are summarized in Table 1.[11] Moreover, due to the initial isotropy we consider the initial conditions as follows:

---

[10] Note that such viscous regularization allows to smoothen the sharp transition between elastic and plastic regions.

$$\boldsymbol{\varepsilon}_{\mathrm{i}}^0 = \boldsymbol{\varepsilon}_{\mathrm{di}}^0 = \boldsymbol{\varepsilon}_{\mathrm{ki}}^0 = \mathbf{0}, \quad s^0 = s_{\mathrm{d}}^0 = 0.$$

The smooth function $\bar{K}^{\mathrm{sat}}(\theta)$ which is needed to compute the overstress $\bar{f}(\vec{y})$ corresponds to the saturated form shown in Fig. 3c. Due to the axial prestrain, the distortion parameter α ranges from 0 up to 0.999993, which corresponds to the (almost) saturated distortional hardening. As it is shown in Fig. 7a, the yield locus undergoes the isotropic expansion, kinematic translation and distortion. The surfaces of constant overstress are depicted in Fig. 7b. In accordance with the modeling assumptions, these surfaces are slightly less distorted than the corresponding yield surface.

Remark 9. Note that the form of the yield surface in the $(\sigma_{11}, \sqrt{3}\sigma_{12})$-space coincides with the boundary of $\mathrm{El}(\bar{K}(\cdot, \alpha))$. This is due to the well-known fact that the scalar product of two symmetric tensors $\boldsymbol{\sigma}_I^{\mathrm{D}}$ and $\boldsymbol{\sigma}_{II}^{\mathrm{D}}$ (where $\boldsymbol{\sigma}_I$ and $\boldsymbol{\sigma}_{II}$ comply with (33)) corresponds to the product of two vectors $\vec{\sigma}_I, \vec{\sigma}_{II} \in \mathbb{R}^2$, defined by $\vec{\sigma}_I := (\sigma_{11}^I, \sqrt{3}\sigma_{12}^I)$, $\vec{\sigma}_{II} := (\sigma_{11}^{II}, \sqrt{3}\sigma_{12}^{II})$. More precisely

$$\boldsymbol{\sigma}_I^{\mathrm{D}} : \boldsymbol{\sigma}_{II}^{\mathrm{D}} = \frac{2}{3}(\sigma_{11}^I \sigma_{11}^{II} + 3\sigma_{12}^I \sigma_{12}^{II}) = \frac{2}{3} \vec{\sigma}_I \cdot \vec{\sigma}_{II}.$$

Therefore, in the context of (33), the angle between two deviatoric stress-states coincides with the angle between two corresponding vectors in the $(\sigma_{11}, \sqrt{3}\sigma_{12})$-space:

$$\arccos\Big(\frac{\boldsymbol{\sigma}_I^{\mathrm{D}} : \boldsymbol{\sigma}_{II}^{\mathrm{D}}}{\|\boldsymbol{\sigma}_I^{\mathrm{D}}\| \; \|\boldsymbol{\sigma}_{II}^{\mathrm{D}}\|}\Big) = \arccos\Big(\frac{\vec{\sigma}_I \cdot \vec{\sigma}_{II}}{\|\vec{\sigma}_I\| \; \|\vec{\sigma}_{II}\|}\Big).$$

Thus, if the form of the saturated yield surface is determined experimentally in the $(\sigma_{11}, \sqrt{3}\sigma_{12})$-space, it can be used to identify the smooth function $\bar{K}^{\mathrm{sat}}(\theta)$.

---

[11] It is not the aim of the current study to identify the material parameters corresponding to the 1100 aluminum alloy. Instead, we validate the material model by the qualitative description of the real experimental data.

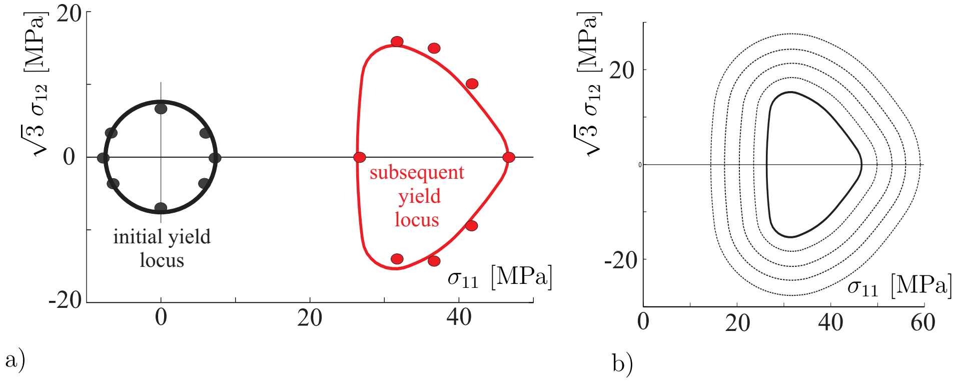

Figure 7: a) Experimental data for annealed 1100 aluminum alloy (Khan et al. , 2010a) and corresponding simulation results, b) Lines of constant overstress f corresponding to plastic anisotropy induced by 2% prestrain in the axial direction.

Table 1: Material parameters used to validate the material model: the viscosity effects are neglected.

k [MPa]	μ [MPa]	c_k [MPa]	c_d [MPa]	γ [MPa]
69000	26000	1010	5000	245

K_0 [MPa]	m [-]	η [s^{-1}]	$\varkappa_\text{k}$ [MPa^{-1}]	$\varkappa_\text{d}$ [MPa^{-1}]	β [-]
7.4	1	0	0.02	0.1	35

If, additionally, the specimen can be loaded by an internal pressure, the hoop stress σ_{22} must be considered, as well:

$$\boldsymbol{\sigma} = \sigma_{11}\mathbf{e}_1 \otimes \mathbf{e}_1 + \sigma_{22}\mathbf{e}_2 \otimes \mathbf{e}_2 + \sigma_{12}(\mathbf{e}_1 \otimes \mathbf{e}_2 + \mathbf{e}_2 \otimes \mathbf{e}_1), \ \ \sigma_{22} \geq 0.$$

We simulate the evolution of the yield surface in the process as follows. Starting from the same isotropic initial state, a 2% prestrain is prescribed in the hoop direction. Thus, a similar plastic anisotropy is introduced, as in the previous case. The form of the yield surface for a fixed axial stress σ_{11} is then represented in the $(\sigma_{22}, \sqrt{3}\sigma_{12})$-space. As it can be seen in Fig. 8, the form and the size of the yield loci for $\sigma_{11} = 5$ MPa, $\sigma_{11} = 10$ MPa, and $\sigma_{11} = 15$ MPa are the same as for $\sigma_{11} = -5$ MPa, $\sigma_{11} = -10$ MPa, and $\sigma_{11} = -15$ MPa, respectively. Similar to the conventional Huber-Mises yield condition, the material yields at larger σ_{22} stresses for positive σ_{11} than for negative σ_{11}.

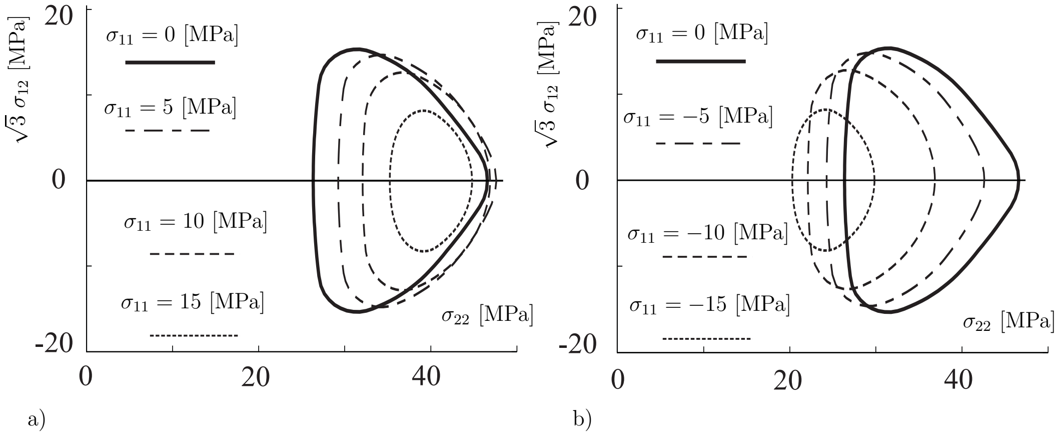

Figure 8: Influence of the axial stress σ_{11} on the form of the yield surface after 2% prestrain in the hoop direction: a) Positive axial stresses; b) Negative axial stresses.

5. Conclusion

A new material model of metal viscoplasticity with an extremely simple structure is presented in the current study. The main modeling assumptions are visualized with the help of a new two-dimensional rheological model. Only second-rank backstress-like tensors are used to capture the path dependent evolution of the plastic anisotropy. Thus, mathematically, the model is not much more complicated than the classical model of Chaboche and Rousselier (1983a,b). At the same time, the proposed technique possess considerable generality and flexibility. No specific form of the saturated yield locus is considered, since *any* smooth convex yield locus can be captured.

An important ingredient of the material modeling is the interpolation between the initial intact yield surface and the saturated one. The interpolation rule proposed in the current study *ensures the convexity* of the yield surface at any stage of hardening. It is shown that this interpolation rule allows to obtain a thermodynamically consistent material model.

The model contains 6 hardening parameters with 2 parameters per hardening type. These parameters posses a clear mechanical interpretation and can be identified experimentally.

Acknowledgement

This research was supported by German Research Foundation (DFG) within SFB 692.

Appendix A

Let us discuss the numerical computation of $\mathcal{D}\big(\vec{y}, \alpha \mathrm{El}^{\mathrm{sat}}\big)$. Suppose that the upper half of the boundary of $\mathrm{El}^{\mathrm{sat}}$ is given by N circular arcs connecting $\vec{y}^{\,i-1}$ and $\vec{y}^{\,i}$ for $i \in \{1, ..., N\}$ as shown in Fig. 9a. The outward normal and the tangent at $\vec{y}^{\,i}$ will be denoted by $\vec{n}^{\,i}$ and $\vec{t}^{\,i}$, respectively. The orientation of the tangent is chosen in such way that the pair $\{\vec{n}^{\,i}, \vec{t}^{\,i}\}$ forms a right-handed corner. In particular, we have

$$\vec{y}^{\,0} = (1, 0), \quad \vec{t}^{\,0} = (0, 1), \quad \vec{t}^{\,N} = (0, -1).$$

For each arc connecting $\vec{y}^{\,i-1}$ and $\vec{y}^{\,i}$ consider its center $\vec{y}_c^{\,i}$ and its radius r^i. In order to make sure that the boundary of $\mathrm{El}^{\mathrm{sat}}$ is smooth, we require

$$\frac{\vec{y}^{\,0} - \vec{y}_c^{\,1}}{r^1} = \vec{n}^{\,0}, \quad \frac{\vec{y}^{\,N} - \vec{y}_c^{\,N}}{r^N} = \vec{n}^{\,N};$$

$$\frac{\vec{y}^{\,i} - \vec{y}_c^{\,i}}{r^i} = \frac{\vec{y}^{\,i} - \vec{y}_c^{\,i+1}}{r^{i+1}} = \vec{n}^{\,i} \text{ for all } i \in \{1, ..., N-1\}.$$

Let $\alpha \in [0, 1]$ and $\vec{y} = \|\vec{y}\|(\cos(\theta), \sin(\theta))$ be given such that $\theta \in [0, \pi]$. The algorithm used to compute the distance $\mathcal{D}\big(\vec{y}, \alpha \mathrm{El}^{\mathrm{sat}}\big)$ is as follows.

- Check the inclusion: If $\|\vec{y}\| \leq \alpha \bar{K}^{\mathrm{sat}}(\theta)$ then $\mathcal{D}\big(\vec{y}, \alpha \mathrm{El}^{\mathrm{sat}}\big) = 0$.
- Otherwise, find the corresponding arc: Find $i \in \{1, ..., N\}$ such that (cf. Fig. 9b)

$$(\vec{y} - \alpha \vec{y}^{\,i-1}) \cdot \vec{t}^{\,i-1} \geq 0, \quad (\vec{y} - \alpha \vec{y}^{\,i}) \cdot (-\vec{t}^{\,i}) \geq 0, \tag{34}$$

$$(\vec{y} - \alpha \vec{y}^{\,i-1}) \cdot \mathbf{Q} \cdot (\vec{y}^{\,i} - \vec{y}^{\,i-1}) \geq 0, \quad \mathbf{Q} := \vec{e}_1 \otimes \vec{e}_2 - \vec{e}_2 \otimes \vec{e}_1. \tag{35}$$

- The distance is then given by

$$\mathcal{D}\big(\vec{y}, \alpha \mathrm{El}^{\mathrm{sat}}\big) = \|\vec{y} - \alpha \vec{y}_c^{\,i}\| - \alpha r^i.$$

Moreover, the outward unit normal is given by

$$\vec{n} = \frac{\partial \bar{f}\big(\vec{y}, \alpha\big)}{\partial \vec{y}} = \frac{\partial \mathcal{D}\big(\vec{y}, \alpha \mathrm{El}^{\mathrm{sat}}\big)}{\partial \vec{y}} = \frac{\vec{y} - \alpha \vec{y}_c^{\,i}}{\|\vec{y} - \alpha \vec{y}_c^{\,i}\|}. \tag{36}$$

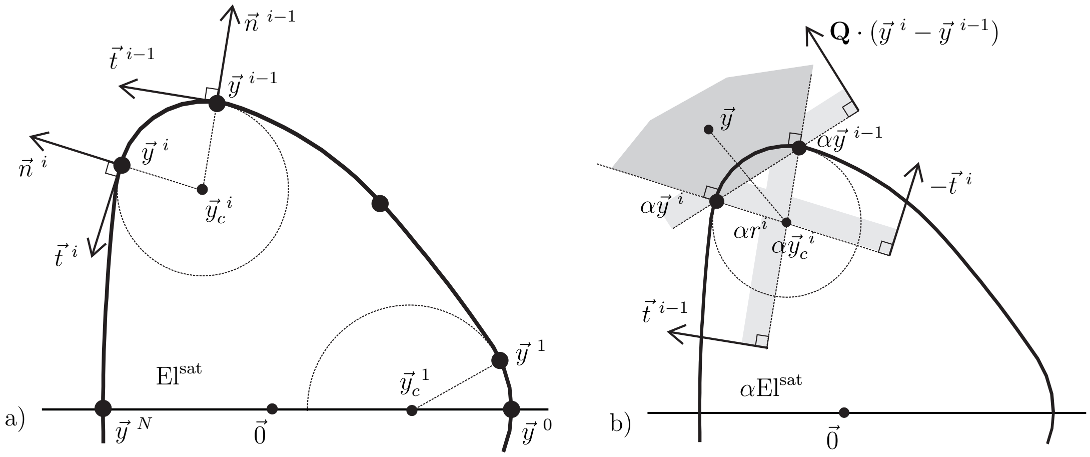

Figure 9: a) A smooth boundary of $\mathrm{El}^{\mathrm{sat}}$ is represented by a sequence of circular arcs. Each circle is characterized by its center $\vec{y}_c^{\,i}$ and radius r^i; b) For a given $\vec{y}$, the inequalities (34), (35) are satisfied within the shaded region. For the suitable i, the distance to $\alpha\mathrm{El}^{\mathrm{sat}}$ is computed as $\mathcal{D}\big(\vec{y},\alpha\mathrm{El}^{\mathrm{sat}}\big)=\|\vec{y}-\alpha\vec{y}_c^{\,i}\|-\alpha r^i$.

Appendix B

Let us discuss the computation of the derivative $\frac{\partial f(\boldsymbol{\sigma})}{\partial\boldsymbol{\sigma}}$, which enters the formulation of the normality rule (23). Suppose $f>0$. Thus, $\boldsymbol{\sigma}^{\mathrm{D}}_{\mathrm{eff}}\neq\mathbf{0}$ and the radial direction $\boldsymbol{R}_{\mathrm{eff}}:=\boldsymbol{\sigma}^{\mathrm{D}}_{\mathrm{eff}}/\|\boldsymbol{\sigma}^{\mathrm{D}}_{\mathrm{eff}}\|$ is well defined. Recall that the hardening variables $\boldsymbol{X}_{\mathrm{k}}$, $\boldsymbol{X}_{\mathrm{d}}$, and R are to be held constant during differentiation. Having this in mind, we get

$$\frac{\partial\|\boldsymbol{\sigma}^{\mathrm{D}}_{\mathrm{eff}}\|}{\partial\boldsymbol{\sigma}}=\frac{\boldsymbol{\sigma}^{\mathrm{D}}_{\mathrm{eff}}}{\|\boldsymbol{\sigma}^{\mathrm{D}}_{\mathrm{eff}}\|}=\boldsymbol{R}_{\mathrm{eff}}. \tag{37}$$

Next, taking into account that $\frac{d\ \arccos(\Phi)}{d\Phi}=-(\sin(\arccos(\Phi)))^{-1}$, we obtain for $\theta\neq 0$

$$\frac{\partial\theta}{\partial\boldsymbol{\sigma}}=\frac{\partial\ \arccos\Big(\frac{\boldsymbol{\sigma}^{\mathrm{D}}_{\mathrm{eff}}\ :\ \boldsymbol{X}_{\mathrm{d}}}{\|\boldsymbol{\sigma}^{\mathrm{D}}_{\mathrm{eff}}\|\ \|\boldsymbol{X}_{\mathrm{d}}\|}\Big)}{\partial\boldsymbol{\sigma}}=-\frac{1}{\sin\theta}\frac{\partial\Big(\frac{\boldsymbol{\sigma}^{\mathrm{D}}_{\mathrm{eff}}\ :\ \boldsymbol{X}_{\mathrm{d}}}{\|\boldsymbol{\sigma}^{\mathrm{D}}_{\mathrm{eff}}\|\ \|\boldsymbol{X}_{\mathrm{d}}\|}\Big)}{\partial\boldsymbol{\sigma}}. \tag{38}$$

Moreover, since $\theta\in[0,\pi]$ is the angle between $\boldsymbol{X}_{\mathrm{d}}$ and $\boldsymbol{R}_{\mathrm{eff}}$, we get

$$\sin\theta=\frac{\|\boldsymbol{X}_{\mathrm{d}}-(\boldsymbol{X}_{\mathrm{d}}:\boldsymbol{R}_{\mathrm{eff}})\boldsymbol{R}_{\mathrm{eff}}\|}{\|\boldsymbol{X}_{\mathrm{d}}\|}.$$

Substituting this result into (38) and taking into account that $\frac{\partial(\boldsymbol{\sigma}^{\mathrm{D}}_{\mathrm{eff}}\,:\,\boldsymbol{X}_{\mathrm{d}})}{\partial\boldsymbol{\sigma}} = \boldsymbol{X}_{\mathrm{d}}$ we get for $\theta \neq 0$

$$\frac{\partial\theta}{\partial\boldsymbol{\sigma}} = -\frac{1}{\|\boldsymbol{\sigma}^{\mathrm{D}}_{\mathrm{eff}}\|}\frac{\boldsymbol{X}_{\mathrm{d}} - (\boldsymbol{X}_{\mathrm{d}} : \boldsymbol{R}_{\mathrm{eff}})\boldsymbol{R}_{\mathrm{eff}}}{\|\boldsymbol{X}_{\mathrm{d}} - (\boldsymbol{X}_{\mathrm{d}} : \boldsymbol{R}_{\mathrm{eff}})\boldsymbol{R}_{\mathrm{eff}}\|}. \tag{39}$$

Further, differentiating (21) we obtain

$$\frac{\partial f(\boldsymbol{\sigma}, \boldsymbol{X}_{\mathrm{k}}, \boldsymbol{X}_{\mathrm{d}}, R)}{\partial\boldsymbol{\sigma}} = \sqrt{\frac{2}{3}}(K_0 + R)\frac{\partial\bar{f}\big(\vec{y}(\|\boldsymbol{\sigma}^{\mathrm{D}}_{\mathrm{eff}}\|, \theta), \alpha\big)}{\partial\boldsymbol{\sigma}}, \tag{40}$$

where

$$\vec{y}(\|\boldsymbol{\sigma}^{\mathrm{D}}_{\mathrm{eff}}\|, \theta) = \frac{\sqrt{3/2}\ \|\boldsymbol{\sigma}^{\mathrm{D}}_{\mathrm{eff}}\|}{K_0 + R}(\cos(\theta), \sin(\theta)). \tag{41}$$

It follows from (41) that

$$\frac{\partial\vec{y}}{\partial\|\boldsymbol{\sigma}^{\mathrm{D}}_{\mathrm{eff}}\|} = \frac{\sqrt{3/2}}{K_0 + R}(\cos(\theta), \sin(\theta)),\ \frac{\partial\vec{y}}{\partial\theta} = \frac{\sqrt{3/2}\ \|\boldsymbol{\sigma}^{\mathrm{D}}_{\mathrm{eff}}\|}{K_0 + R}(-\sin(\theta), \cos(\theta)). \tag{42}$$

Next, note that the degree of distortion α is to be held constant as well, since it is a unique function of $\boldsymbol{X}_{\mathrm{d}}$. Thus, using the chain rule we get from (40)

$$\frac{\partial f(\boldsymbol{\sigma}, \boldsymbol{X}_{\mathrm{k}}, \boldsymbol{X}_{\mathrm{d}}, R)}{\partial\boldsymbol{\sigma}} = \sqrt{\frac{2}{3}}(K_0 + R)\Bigg[\bigg(\frac{\partial\bar{f}(\vec{y}, \alpha)}{\partial\vec{y}} \cdot \frac{\partial\vec{y}}{\partial\|\boldsymbol{\sigma}^{\mathrm{D}}_{\mathrm{eff}}\|}\bigg)\frac{\partial\|\boldsymbol{\sigma}^{\mathrm{D}}_{\mathrm{eff}}\|}{\partial\boldsymbol{\sigma}} + \bigg(\frac{\partial\bar{f}(\vec{y}, \alpha)}{\partial\vec{y}} \cdot \frac{\partial\vec{y}}{\partial\theta}\bigg)\frac{\partial\theta}{\partial\boldsymbol{\sigma}}\Bigg].$$

Substituting (37), (39), and (42) into this result we get for $\theta \neq 0$

$$\frac{\partial f(\boldsymbol{\sigma}, \boldsymbol{X}_{\mathrm{k}}, \boldsymbol{X}_{\mathrm{d}}, R)}{\partial\boldsymbol{\sigma}} = \Big(\frac{\partial\bar{f}(\vec{y}, \alpha)}{\partial\vec{y}} \cdot (\cos(\theta), \sin(\theta))\Big)\boldsymbol{R}_{\mathrm{eff}} + \Big(\frac{\partial\bar{f}(\vec{y}, \alpha)}{\partial\vec{y}} \cdot (\sin(\theta), -\cos(\theta))\Big)\frac{\boldsymbol{X}_{\mathrm{d}} - (\boldsymbol{X}_{\mathrm{d}} : \boldsymbol{R}_{\mathrm{eff}})\boldsymbol{R}_{\mathrm{eff}}}{\|\boldsymbol{X}_{\mathrm{d}} - (\boldsymbol{X}_{\mathrm{d}} : \boldsymbol{R}_{\mathrm{eff}})\boldsymbol{R}_{\mathrm{eff}}\|}. \tag{43}$$

Here, the gradient of the non-dimensional overstress is computed by (36). Finally, the normality vector tends to the radial direction as $\theta \to 0$. Therefore

$$\frac{\partial f(\boldsymbol{\sigma}, \boldsymbol{X}_{\mathrm{k}}, \boldsymbol{X}_{\mathrm{d}}, R)}{\partial\boldsymbol{\sigma}} = \boldsymbol{R}_{\mathrm{eff}} \quad \text{for } \theta = 0.$$

References

Annin, B.D., 1978. Experimental investigation of plastic properties under complex loadings (In Russian). Mechanika tverdogo tela, 347-351.

Aretz, H., 2008. A simple isotropic-distortional hardening model and its application in elastic-plastic analysis of localized necking in orthotropic sheet metals. International Journal of Plasticity, **24**, 1457-1480.

Baltov, A., Sawczuk, A., 1964. A rule of anisotropic hardening. Acta Mechanika, **1**(2), 81-92.

Barlat, F., Gracio, J.J., Lee, M.G., Rauch, E.F., Vincze, G. 2011. An alternative to kinematic hardening in classical plasticity. International Journal of Plasticity, **27**, 1309-1327.

Betten, J., 1976. Plastische Anisotropie und Bauschinger-Effekt; allgemeine Formulierung und Vergleich mit experementell ermittelten Fließortkurven. Acta Mechanika, **25**, 79-94.

Chaboche, J.L., Rousselier, G., 1983a. On the plastic and viscoplastic constitutive equations, part 1: Rules developed with internal variable concept. Journal of Pressure Vessel Technology, **105**, 153 - 158.

Chaboche, J.L., Rousselier, G., 1983b. On the plastic and viscoplastic constitutive equations, part 2: Application of internal variable concept to the 316 stainless steel. Journal of Pressure Vessel Technology, **105**, 159 - 164.

Dafalias, Y.F., Popov, E.P., 1975. A model of nonlinearly hardening materials for complex loading. Acta Mechanica, **21**, 173–192.

Dafalias, Y.F., 1979. Anisotropic hardening of initially orthotropic materials. ZAMM, **59**, 437–446.

Dafalias, Y.F., Schick, D., Tsakmakis, C. 2002. A simple model for describing yield surface evolution. Lecture note in applied and computational mechanics, K. Hutter and H. Baaser, eds., Springer, Berlin, 169–201.

Dafalias, Y.F., Feigenbaum, H.P. 2011. Directional distortional hardening in plasticity within thermodynamics. In: Recent Advances in Mechanics, 61–78.

Danilov, V., 1971. On the formulation of the law of distortional hardening (In Russian). Mechanika tverdogo tela **6**, 146-150.

Dannemeyer, S., 1999. Zur Veränderung der Fließfläche von Baustahl bei mehrachsiger plastischer Wechselbeanspruchung. Braunschweig (Carolo-Wilhelmina University).

Fang, L., Qiang, F., Cen, C., Naigang, L., 2011. An elasto-plastic damage constitutive theory and its prediction of evolution of subsequent yield surfaces and elastic constants. International Journal of Plasticity, **27**, 1355-1383.

Feigenbaum, H.P., Dafalias, Y.F., 2007. Directional distortional hardening in metal plasticity within thermodynamics. International Journal of Solids and Structures, **44**, 7526-7542.

Feigenbaum, H.P., Dafalias, Y.F., 2008. Simple model for directional distortional hardening in metal plasticity within thermodynamics. Journal of Engineering Mechanics, **134** 9, 730-738.

François, M., 2001. A plasticity model with yield surface distortion for non proportional loading. International Journal of Plasticity, **17**, 703–717.

Freund, M., Shutov, A.V., Ihlemann, J., 2011. Simulation of distortional hardening by generalizing a uniaxial model of finite strain viscoplasticity. Submitted to International Journal of Plasticity.

Grewolls, G., Kreißig, R., 2001. Anisotropic hardening – numerical application of a cubic yield theory and consideration of variable r-values for sheet metal. European Journal of Mechanics A/Solids, **20**, 585–599.

Hashiguchi, K., 1989. Subloading surface model in unconventional plasticity. Int. J. Solids Structures, **25**,8, 917–945.

Haupt, P., 2002. Continuum Mechanics and Theory of Materials, 2nd edition, Springer.

Helling, D.E., Miller, A.K., 1987. The incorporation of yield surface distortion into a unified constitutive model, Part 1: equation development. Acta Mechanika **69**, 9–23.

Helm, D., 2001. Formgedächtnislegierungen, experimentelle Untersuchung, phänomenologische Modellierung und numerische Simulation der thermomechanischen Materialeigenschaften (Universitätsbibliothek Kassel).

Henann, D.L., Anand, L., 2009. A large deformation theory for rate–dependent elastic-plastic materials with combined isotropic and kinematic hardening. International Journal of Plasticity 25, 1833-1878.

Hill, R., 1948. A theory of the yielding and plastic flow of anisotropic metals. Proceedings Royal Society (London), Series A **193**, 281-297.

Ilyushin, A.A., 1954. On the relation between stresses and small strains in the mechanics of continua (In Russian). Prikl. Mat. Mech. **18**, 641–666.

Itskov, M., 2007. Tensor Algebra and Tensor Analysis for Engineers: With Applications to Continuum Mechanics (Springer).

Khan, A.S., Pandey, A., Stoughton, T., 2010a. Evolution of subsequent yield surfaces and elastic constants with finite plastic deformation. Part II: A very high work hardening aluminum alloy (annealed 1100 Al). International Journal of Plasticity 26, 1421-1431.

Khan, A.S., Pandey, A., Stoughton, T., 2010b. Evolution of subsequent yield surfaces and elastic constants with finite plastic deformation. Part III: Yield surface in tension-tension stress space (Al 6061T 6511 and annealed 1100 Al). International Journal of Plasticity 26, 1432-1441.

Kowalsky, U., Ahrens, H., Dinkler, D., 1999. Distorted yield surfaces modelling by higher order anisotropic hardening tensors. Comput. Mater. Sci. **16**, 81-88.

Kurtyka, T., Zyczkowski, M., 1985. A geometric description of distortional plastic hardening of deviatoric materials. Arch. Mech., **37**, 383 – 395.

Kurtyka, T., Zyczkowski, M., 1996. Evolution equations for distortional plastic hardening. International Journal of Plasticity, **12**, 191 – 213.

Lion, A., 2000. Constitutive modelling in finite thermoviscoplasticity: a physical approach based on nonlinear rheological elements. International Journal of Plasticity, **16**, 469–494.

Noman, M., Clausmeyer, T., Barthel, C., Svendsen, B., Huétink, J., Riel, M., 2010. Experimental characterization and modeling of the hardening behavior of the sheet steel LH800. Materials Science and Engineering A **527**, 2515-2526.

Ortiz, M., Popov, E.P., 1983. Distortional hardening rules for metal plasticity. J. Engng Mech., 109, 1042 – 1058.

Palmow, W.A., 1984. Rheologische Modelle für Materialien bei endlichen Deformationen. Technische Mechanik, 4, 20–31.

Panhans, S., 2006. Ein viskoplastisches Materialmodell mit nichtquadratischer Fließfunktion. PhD thesis, (TU Chemnitz).

Panhans, S., Kreißig, R., 2006. A viscoplastic material model of overstress type with a non-quadratic yield function. European Journal of Mechanics A/Solids, **25**, 283–298.

Perzyna, P., 1963. The constitutive equations for rate sensitive plastic materials. Quarterly of Applied Mathematics, **20** 321–331.

Petrov, M.G., 1998. Rheological properties of materials from the point of view of physical kinetics. Journal of Applied Mechanics and Technical Physics, **39** 1, 104–112.

Pietryga, M.P., Vladimirov, I.N., Reese, S., 2012. A finite deformation model for evolving flow anisotropy with distortional hardening including experimental validation. Mechanics of Materials, **44**, 163-173.

Plesek, J., Feigenbaum, H.P., Dafalias, Y.F., 2010. Convexity of yield surface with directional distortional hardening rules. Journal of Engineering Mechanics, **136** 4, 477–484.

Prager, W., 1935. Der Einfluß der Verformung auf die Fließbedingung zähplastischer Körper. ZAMM, **15** 1/2, 76–80.

Rees, D.W.A., 1984. An examination of yield surface distortion and translation. Acta Mechanica, **52** 15–40.

Rousselier, G., Barlat, F., Yoon, J.W., 2010. A novel approach for anisotropic hardening modeling. Part II: Anisotropic hardening in proportional and non-proportional loadings, application to initially isotropic material. International Journal of Plasticity, **26** 1029–1049.

Steck, E., Ritter, R., Peil, U., Ziegenbein A., 2001. Deutsche Forschungsgemeinschaft, Plasticity of Materials: Experiments, Models, Computation. (Wiley-VCH Verlag GmbH).

Shutov, A.V., Kreißig, R., 2008a. Finite strain viscoplasticity with nonlinear kinematic hardening: Phenomenological modeling and time integration. Computer Methods in Applied Mechanics and Engineering, **197**, 2015–2029.

Shutov, A.V., Kreißig, R., 2008b. Application of a coordinate-free tensor formalism to the numerical implementation of a material model. ZAMM, **88** 11, 888–909.

Shutov, A.V., Kreißig, R., 2010. Regularized strategies for material parameter identification in the context of finite strain plasticity. Technische Mechanik, **30** 1-3, 280–295.

Shutov, A.V., Panhans, S., Kreißig, R., 2011. A phenomenological model of finite strain viscoplasticity with distortional hardening. ZAMM, **91** 8, 653–680.

Shutov, A.V., Ihlemann, J., 2011. On the simulation of plastic forming under consideration of thermal effects. Materialwissenschaft und Werkstofftechnik, **42** 7, 632–638.

Streilein, T., 1997. Erfassung formativer Verfestigung in viskoplastischen Stoffmodellen. PhD thesis, Bericht Nr. 97/83 (TU Braunschweig).

Viatkina, E.M., 2005. Micromechanical modelling of strain path dependency in FCC metals. Technische Universiteit Eindhoven, Eindhoven.

Viatkina, E.M., Brekelmans, W.A.M., Geers, M.G.D., 2007. Modelling the evolution of dislocation structures upon stress reversal. International Journal of Solids and Structures, 44, 6030-6054.

Vladimirov, I.N., Pietryga, M.P., Reese, S., 2010. Anisotropic finite elastoplasticity with nonlinear kinematic and isotropic hardening and application to sheet metal forming. International Journal of Plasticity, **26**, 659–687.

Wegener, K., Schlegel, M., 1996. Suitability of yield functions for the approximation of subsequent yild surfaces. International Journal of Plasticity, **12**, 1151 – 1177.